A Causal View on Compositional Data

Elisabeth Ailer
Helmholtz AI, Munich

Christian L. Müller
Ludwig Maximilian University
Helmholtz Zentrum Munich
Flatiron Institute, New York

Niki Kilbertus
Technical University of Munich
Helmholtz AI, Munich

Abstract

Many scientific datasets are compositional in nature. Important examples include species abundances in ecology, rock compositions in geology, topic compositions in large-scale text corpora, and sequencing count data in molecular biology. Here, we provide a causal view on compositional data in an instrumental variable setting where the composition acts as the cause. First, we crisply articulate potential pitfalls for practitioners regarding the interpretation of compositional causes from the viewpoint of interventions and warn against attributing causal meaning to common summary statistics such as diversity indices. We then advocate for and develop multivariate methods using statistical data transformations and regression techniques that take the special structure of the compositional sample space into account. In a comparative analysis on synthetic and real data we show the advantages and limitations of our proposal. We posit that our framework provides a useful starting point and guidance for valid and informative cause-effect estimation in the context of compositional data.

1 Introduction

The statistical modeling of compositional (or relative abundance) data plays a pivotal role in many areas of science, ranging from the analysis of mineral samples or rock compositions in earth sciences (Aitchison, 1982) to correlated topic modeling in large text corpora (Blei & Lafferty, 2005, 2007). Recent advances in biological high-throughput sequencing techniques, including single-cell RNA-Seq and microbial amplicon sequencing (Rozenblatt-Rosen et al., 2017; Turnbaugh et al., 2007), have triggered renewed interest in compositional data analysis. Since only a limited total number of transcripts can be captured in a sample, the resulting count data provides relative abundance information about the occurrences of mRNA transcripts or microbial amplicon sequences, respectively (Quinn et al., 2018; Gloor et al., 2017). When relative abundances are normalized by their respective totals, the resulting *compositional data* comprises the proportions of some whole, implying that data points live on the unit simplex $\mathbb{S}^{p-1} := \{x \in \mathbb{R}^{p}_{\geq 0} \mid \sum_{j=1}^{p} x_j = 1\}$.

For example, assume p distinct nutrients can be present in agricultural soil in different geographical regions. A specific soil sample is then represented by a vector x, where x_j denotes the relative abundance of nutrient j (under an arbitrary ordering of nutrients). An increase in x_1 within this composition could correspond to an actual increase in the absolute abundance of the first nutrient while the rest remained constant. However, it could equally result from a decrease of the first nutrient with the remaining ones having decreased even more. This property renders interpretability in compositional data analysis challenging, especially for causal queries: how does the relative abundance of a certain nutrient affect soil fertility?

Statisticians have recognized the significance of compositional data early on (dating back to Karl Pearson) and tailored models to naturally account for compositionality via simplex arithmetic (Aitchison, 1982). Despite these efforts, adjusting modern machine learning methods to compositional data remains an active field of research (Rivera-Pinto et al., 2018; Cammarota et al., 2020; Quinn et al., 2020; Oh & Zhang, 2020).

This work focuses on estimating the causal effect of a composition on a categorical or continuous outcome. Let us motivate this problem further with a human microbiome example. The *human microbiome* is the collection of microbes in and on the human body. It comprises roughly as many cells as the body has human cells (Sender et al., 2016) and is thought to play a crucial role in health and disease ranging from obesity to allergies, mental disorders, Type-2 diabetes, and cancer (Cho & Blaser, 2012; Clemente et al., 2012; Pflughoeft & Versalovic, 2012; Shreiner et al., 2015; Lynch & Pedersen, 2016). As contemporary microbiome datasets rapidly grow in size and fidelity, they harbor great potential to substantially improve our understanding of such conditions. Experimental work, predominantly in mice studies, provides strong evidence for a potentially causal role of the gut microbiome on health-related outcomes, such as obesity (Cho et al., 2012; Mahana et al., 2016; Schulfer et al., 2019). Only recently have the fundamental challenges in interpreting causal effects of compositions been acknowledged explicitly (Arnold et al., 2020; Breskin & Murray, 2020) with little work on how to estimate such effects from observational data.

One major hurdle in answering such causal questions are potential unobserved confounders. The human microbiome co-evolves with its host and the external environment, for example through diet, activity, climate, or geography, leading to plentiful microbiome-host-environment interactions (Vujkovic-Cvijin et al., 2020). Carefully designed studies may allow us to control for certain environmental factors and specifics of the host. Two recent works studied the causal mediation effect of the microbiome on health-related outcomes, assuming all relevant covariates are observed and can be controlled for (Sohn & Li, 2019; Wang et al., 2020). However, in practice there is little hope of measuring *all* latent factors in these complex interactions. The cause-effect estimation task is thus fundamentally limited by *unobserved confounding*.

More specifically, without further assumptions, the direct causal effect $X \to Y$ is not identified from observational data in the presence of unobserved confounding $X \leftarrow U \to Y$ (Pearl, 2009).[1] One common way to nevertheless identify the causal effect from purely observational data is through so-called instrumental variables (Angrist & Pischke, 2008). An *instrumental variable Z* is a variable that has an effect on the cause X ($Z \to X$), but is independent of the confounder ($Z \perp\!\!\!\perp U$), and conditionally independent of the outcome given the cause and the confounders ($Z \perp\!\!\!\perp Y \,|\, \{U, X\}$). In practice, it can be hard to find valid instruments for a target effect (Hernán & Robins, 2006), but when they do exist, instrumental variables often render efficient cause-effect estimation possible.

In this work, we develop methods to estimate the direct causal effect of a *compositional cause* on a continuous or categorical outcome within the instrumental variable setting. Our first contribution is a thorough exploration of how to interpret compositional causes, including an argument for why it is misleading to assign causal meaning to common summary statistics of compositions such as α-diversity in the realm of microbiome data or ecology. These findings motivate our in-depth analysis of two-stage methods for compositional treatments that allow for cause-effect estimation of individual relative abundances on the outcome. A key focus in this analysis lies on misspecification as a major obstacle to interpretable effect

---

[1] We typically interpret upper-case letters such as X as random variables and use lower-case letters such as $x \in \mathbb{S}^{p-1}$ for a specific realization of X.

estimates. After our theoretical considerations, we evaluate the efficacy and robustness of our proposed method empirically on both synthetic as well as real data from a mouse experiment examining how the gut microbiome affects body weight instrumented by sub-therapeutic antibiotic treatment (STAT). [2]

2 Background and setup

2.1 Compositional data analysis

Simplex geometry. Aitchison (1982) introduced the *perturbation* and *power transformation* as the simplex $\mathbb{S}^{p-1}$ counterparts to addition and scalar multiplication of Euclidean vectors in $\mathbb{R}^p$:

Perturbation	Power transformation
$\oplus : \mathbb{S}^{p-1} \times \mathbb{S}^{p-1} \to \mathbb{S}^{p-1}$	$\odot : \mathbb{R} \times \mathbb{S}^{p-1} \to \mathbb{S}^{p-1}$
$x \oplus w = C(x_1 w_1, \ldots, x_p w_p)$	$a \odot x := C(x_1^a, x_2^a, \ldots, x_p^a)$

Here, the *closure operator* $C : \mathbb{R}_{\geq 0}^p \to \mathbb{S}^{p-1}$ normalizes a p-dimensional, non-negative vector to the simplex $C(x) := x / \sum_{i=1}^p x_i$. Together with the dot-product

$$\langle x, w \rangle := \frac{1}{2p} \sum_{i,j=1}^p \log\left(\frac{x_i}{x_j}\right) \log\left(\frac{w_i}{w_j}\right)$$

the tuple $(\mathbb{S}^{p-1}, \oplus, \odot, \langle \cdot, \cdot \rangle)$ forms a finite-dimensional real Hilbert space (Pawlowsky-Glahn & Egozcue, 2001) allowing to transfer usual geometric notions such as lines and circles from Euclidean space to the simplex.

Coordinate representations. The p entries of a composition remain dependent via the unit sum constraint, leading to $\mathbb{S}^{p-1}$ having dimension $p - 1$. To deal with this fact, different invertible log-based transformations have been proposed, for example the additive log ratio, centered log ratio (Aitchison, 1982), and isometric log ratio (Egozcue et al., 2003) transformations

$$\text{alr}(x) = V_a \log(x), \quad \text{clr}(x) = V_c \log(x), \quad \text{ilr}(x) = V_i \log(x),$$

where the logarithm is applied element-wise and the matrices $V_a, V_i \in \mathbb{R}^{(p-1) \times p}$ and $V_c \in \mathbb{R}^{p \times p}$ are defined in Appendix A. While alr is a vector space isomorphism that preserves a one-to-one correspondence between all components except for one, which is chosen as a fixed reference point to reduce the dimensionality (we choose x_p, but any other component works), it is not an isometry, i.e., it does not preserve distances or scalar products. Both clr and ilr are also isometries, but clr only maps onto a subspace of $\mathbb{R}^p$, which often renders measure theoretic objects such as distributions degenerate. As an isometry between $\mathbb{S}^{p-1}$ and $\mathbb{R}^{p-1}$, ilr allows for an orthonormal coordinate representation of compositions. However, it is hard to assign meaning to the individual components of ilr(x), which all entangle a different subset of relative abundances in x leading to challenges for interpretability (Greenacre & Grunsky, 2019). Therefore, alr remains a useful tool despite its arguably inferior theoretical properties.

Log-contrast estimation. The key advantage of such coordinate transformations is that they allow us to use regular multivariate data analysis methods (typically tailored to Euclidean

---

[2]The code is available on `https://github.com/EAiler/comp-iv`.

space) for compositional data. For example, we can directly fit a linear model $y = \beta_0 + \beta^T \operatorname{ilr}(x) + \epsilon$ on the ilr coordinates via ordinary least squares (OLS) regression. However, in real-world datasets, p is often a large number capturing "all possible components in a measurement", leading to $p \gg n$ with each of the n measurements being sparse, i.e., a substantial fraction of x being zero. This overparameterization calls for regularization. The problem with enforcing sparsity in a "linear-in-ilr" model is that a zero entry in β does not correspond directly to a zero effect of the relative abundance of any single taxon. This motivates *log-contrast* estimation (Aitchison & Bacon-Shone, 1984) for the $p > n$ setting with a sparsity penalty (Lin et al., 2014; Combettes & Müller, 2020)

$$\min_\beta \sum_{i=1}^n \mathcal{L}(x_i, y_i, \beta) + \lambda \|\beta\|_1 \quad \text{s.t.} \sum_{i=1}^p \beta_i = 0 \,. \tag{1}$$

In our examples, we focus mostly on continuous $y \in \mathbb{R}$ and the squared loss $\mathcal{L}(x, y, \beta) = (y - \beta^T \log(x))^2$. However, our framework in Section 4 also supports the Huber loss for robust Lasso regression as well as an optional joint concomitant scale estimation for both losses. Moreover, for classification tasks with $y \in \{0, 1\}$, we can directly use the squared Hinge loss (or a "Huberized" version thereof) for $\mathcal{L}$, see Appendix E for details. Even though, due to the additional sum constraint, individual components of β are still not—and can never be—entirely disentangled.

Logs and zeros. In the previous paragraphs, we introduced multiple log-based coordinate representations for compositions and claimed at the same time that they often live in the $p \gg n$ setting with sparse measurements. Since the logarithm is undefined for zero entries, a simple strategy is to add a small constant to all absolute counts, so called *pseudo-counts*, which we also use in this work. These pseudo-counts are particularly popular in the microbiome literature where there are many more possible taxa (up to tens of thousands) than occur in any givens sample. The additive constant is often chosen in an ad-hoc fashion, for example 0.5 (Kaul et al., 2017; Lin & Peddada, 2020).

Summary statistics. Traditionally, interpretability issues around compositions have been circumvented by focusing on summary statistics instead of individual relative abundances. One of the key measures to describe ecological populations is *diversity*. Diversity captures the variation within a composition and is in this context often called α-diversity. There is no unique definition of α-diversity. Among the most common ones in the literature are *richness*[3] $\|x\|_0$, *Shannon diversity* $-\sum_{j=1}^p x_j \log(x_j)$ and *Simpson diversity* $-\sum_{j=1}^p x_j^2$. Especially in the microbial context, there exist entire families of diversity measures taking into account species, functional, or phylogenetic similarities between taxa and tracing out continuous parametric profiles for varying sensitivity to highly-abundant taxa. See for example (Leinster & Cobbold, 2012; Chao et al., 2014; Daly et al., 2018) for an overview of the possibilities and choices of estimating α-diversity in a specific application. Given the popularity of α-diversity for assessing the impact and health of microbial compositions (Bello et al., 2018), it appears natural to formulate causal queries generally in terms of summary statistics. In Section 3 we show why we should not assign causal powers to summary statistics.

2.2 Instrumental variables

We briefly recap the assumptions of the instrumental variable setting as depicted in Figure 1. For an *outcome* (or *effect*) Y, a *treatment* (or *cause*) X, and potential *unobserved confounders* U, we assume access to a discrete or continuous *instrument* $Z \in \mathbb{R}^q$ satisfying (i) $Z \perp\!\!\!\perp U$ (the

---

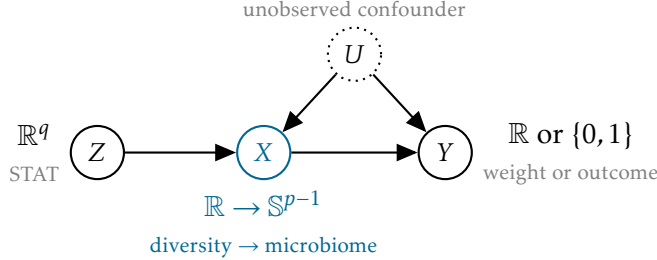[3]We write $\|x\|_0$ for the number of non-zero entries of x and note that this not a norm.

Figure 1: Estimation of the direct causal effect $X \to Y$ via an instrumental variable Z for compositional X with X being represented by a summary statistic or by the entire composition.

confounder is independent of the instrument), (ii) $Z \not\perp\!\!\!\perp X$ ("the instrument influences the cause"), and (iii) $Z \perp\!\!\!\perp Y \,|\, \{X, U\}$ ("the instrument influences the outcome only through the cause"). Our goal is to estimate the direct causal effect of X on Y, written as $\mathbb{E}[Y | do(x)]$ in the do-calculus notation (Pearl, 2009) or as $\mathbb{E}[Y(x)]$ in the potential outcome framework (Imbens & Rubin, 2015), where $Y(x)$ denotes the potential outcome for treatment value x. The functional dependencies are $X = g(Z, U)$, $Y = f(X, U)$. While Z, X, Y denote random variables, we also consider a dataset of n i.i.d. samples $\mathcal{D} = \{(z_i, x_i, y_i)\}_{i=1}^{n}$ from their joint distribution. We collect these datapoints into matrices or vectors denoted by $\boldsymbol{X} \in \mathbb{R}^{n \times p}$ or $\boldsymbol{X} \in (\mathbb{S}^{p-1})^n$, $\boldsymbol{Z} \in \mathbb{R}^{n \times q}$, $\boldsymbol{y} \in \mathbb{R}^n$.

Without further restrictions on f and g, the causal effect is not identified (Pearl, 1995; Bonet, 2001; Gunsilius, 2018). The most common assumption leading to identification is that of *additive noise*, namely $Y = f(X) + U$ with $\mathbb{E}[U] = 0$ and $X \not\perp\!\!\!\perp U$. Here, we overload the symbols f and g for simplicity. The implied Fredholm integral equation of first kind $\mathbb{E}[Y|Z] = \int f(x) \, dP(X|Z)$ is generally ill-posed. Under certain regularity conditions it can be solved consistently even for non-linear f, see e.g., (Newey & Powell, 2003; Blundell et al., 2007) and more recently (Singh et al., 2019; Muandet et al., 2019; Zhang et al., 2020).

Linear case. When $X \in \mathbb{R}^p$ and f, g are linear, the standard *instrumental variable estimator* is

$$\hat{\beta}_{\text{iv}} = (\boldsymbol{X}^T \boldsymbol{P_Z} \boldsymbol{X})^{-1} \boldsymbol{X}^T \boldsymbol{P_Z} \boldsymbol{y} \tag{2}$$

with $\boldsymbol{P_Z} = \boldsymbol{Z}(\boldsymbol{Z}^T \boldsymbol{Z})^{-1} \boldsymbol{Z}^T$. For the *just-identified* case $q = p$ as well as the over-identified case $q > p$, this estimator is consistent and asymptotically unbiased, albeit not unbiased. In the *under-identified* case $q < p$, where there are fewer instruments than treatments, the orthogonality of Z and U does not imply a unique solution. The estimator $\hat{\beta}_{\text{iv}}$ can also be interpreted as the outcome of a *two-stage least squares* (2SLS) procedure consisting of (1) regressing $\boldsymbol{X}$ on $\boldsymbol{Z}$ via OLS $\hat{\delta} = (\boldsymbol{Z}^T \boldsymbol{Z})^{-1} \boldsymbol{Z}^T \boldsymbol{X}$, and (2) regressing $\boldsymbol{y}$ on the predicted values $\hat{\boldsymbol{X}} = \boldsymbol{Z}\hat{\delta}$ via OLS, again resulting in $\hat{\beta}_{\text{iv}}$. Practitioners are typically discouraged from using the manual two-stage approach, because the OLS standard errors of the second stage are wrong—a correction is needed (Angrist & Pischke, 2008).

Moreover, the two-stage description suggests that the two stages are independent problems and thereby seems to invite us to mix and match different regression methods as we see fit. Angrist & Pischke (2008) highlight that the asymptotic properties of $\hat{\beta}_{\text{iv}}$ rely on the fact that for OLS the residuals of the first stage are uncorrelated with $\hat{\beta}_{\text{iv}}$ and the instruments $\boldsymbol{Z}$. Hence, for OLS we achieve consistency *even when the first stage is misspecified*. For a non-linear first stage regression we may only hope to achieve uncorrelated residuals asymptotically when the model is correctly specified. Replacing the OLS first stage with a non-linear model

is known as the "forbidden regression", a term commonly attributed to Prof. Jerry Hausmann. Angrist and Pischke acknowledge that the practical relevance of the forbidden regression is not well understood. Starting with Kelejian (1971) there is now a rich literature on the circumstances under which "manual 2SLS" with non-linear first (and/or second) stage can yield consistent causal estimators. Primarily interested in high-dimensional, compositional X, we cannot directly use OLS for either stage. Hence we pay great attention to potential issues due to the "forbidden regression" and misspecification in our proposed methods. Because we aim for interpretable causal effect estimates, where we want to control the second stage $X \rightarrow Y$ regression, we still concentrate on two-stage methods despite their potential drawbacks.

3   Why compositions?

For some causal queries with compositional treatments it is clear that we are seeking to quantify the causal effect of individual relative abundances: "What is the causal effect of one specific nutrient abundance in the soil composition on fertility?" However, in other domains, it has become customary to avoid the intricacies of compositional data in causal estimation by only considering scalar summary statistics *a priori*. This section has two goals: (a) It explains why, even in situations where summary statistics appear to be useful proxies, no causal conclusions can be drawn from them. (b) Alongside these arguments, we also introduce a real-world dataset (which we return to in Section 4.4) and relevant instrumental variable methods.

We take microbial ecology and microbiome research as an example. There, species diversity became the center of attention to an extent that asking "what is the causal effect of *the diversity* of a composition X on the outcome Y?" appears more intuitive than asking for the causal effect of individual abundances.[4] In fact, popular books and research articles alike seem to suggest that (bio-)diversity is indeed an important *causal driver* of ecosystem functioning and human health, even though these claims are largely grounded in observational, non-experimental data (Chapin et al., 2000; Blaser, 2014). Since α-diversity is described by a real scalar ($p = 1$), if there is an instrumental variable available we are in the just- or over-identified setting and can thus attempt to directly interpret $\hat{\beta}_{iv} \in \mathbb{R}$ in this scenario. The "causal effect" formally is $\mathbb{E}[Y|do(\alpha)]$, the expected value of Y under an *intervention on the diversity*, i.e., externally setting it to the value α with all host and environmental factors unchanged. Our estimate for $\mathbb{E}[Y|do(\alpha)]$ is given by $\hat{\beta}_{iv}\alpha$ (up to an intercept). Critically, this estimand presupposes that for fixed unobserved factors, the outcome *only* depends on the diversity of a composition, and none of the individual abundances. For example, most common diversity measures are invariant under permutation of components and we would have to conclude that all $p!$ permutations of a composition x are equivalent. Even worse, for each value of α, there is a $(p-2)$-dimensional subspace of $\mathbb{S}^{p-1}$ with that diversity. Using diversity as a causal driver forces us to conclude that the outcome is entirely agnostic to all these $p-2$ continuous degrees of freedom. *Hence, assigning causal powers to diversity by estimating $\mathbb{E}[Y|do(\alpha)]$ is highly ambiguous and does not carry the intended meaning.*

In addition to this main pitfall, concerns have been raised about the ambiguity in measuring α-diversity in the first place (Willis, 2019; Shade, 2017; Gloor et al., 2017). Indeed, Figure 2 shows that on a real dataset (see below), different ways of computing diversity may lead to opposite causal effects. The chosen definition of α-diversity has a critical effect on the inferred causal direction, leading to the contradictory conclusions: "A higher α-diversity

---

[4]We note that our arguments apply equally to other domains and scalar summary statistics.
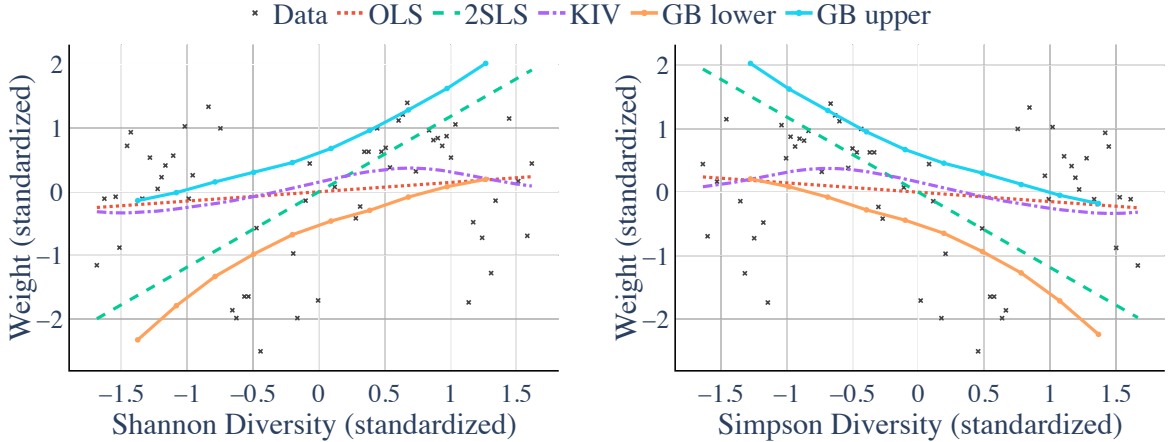
Figure 2: Effect estimates of gut microbiome diversity on body weight using IV methods with different sets of assumptions for Shannon diversity (left) and Simpson diversity (right). All methods are broadly in agreement for each diversity measure separately. However, the effects have opposite sign for Shannon and Simpson diversity leading to inconclusive overall results.

causes weight loss resp. weight gain of the host". We now describe the experimental setup as well as the cause-effect estimation methods used before returning to these results.

Real data. We found the dataset described by Schulfer et al. (2019) to be a good fit for our setting. A total of 57 new born mice were assigned randomly to a sub-therapeutic antibiotic treatment (STAT) during their early stages of development. After 21 days, the gut microbiome composition of each mouse was recorded. We are interested in the causal effect of the gut microbiome composition $X \in \mathbb{S}^{p-1}$ on body weight $Y \in \mathbb{R}$ of the mice (at sacrifice). The random assignment of the antibiotic treatment ensures independence of potential confounders such as genetic factors ($Z \perp\!\!\!\perp U$). The sub-therapeutic dose implies that antibiotics can not be detected in the mice' blood, providing reason to assume no effect of the antibiotics on the weight other than through its effect on the gut microbiome ($Z \perp\!\!\!\perp Y \mid \{U, X\}$).[5] Finally, we observe empirically, that there are statistically significant differences of microbiome compositions between the treatment and control groups ($Z \not\!\perp\!\!\!\perp X$). Thus, the sub-therapeutic antibiotic treatment is a good candidate for an instrument $Z \in \{0, 1\}$ in estimating the effect $X \to Y$.

Methods for one-dimensional causes. We compare the following methods with gradually weakened assumptions to ensure the validity of our cause-effect estimates (see Appendix B for details):

1. *2SLS:* The standard estimator from eq. (2)

2. *KIV:* (Kernel Instrumental Variables): Singh et al. (2019) relax the linearity assumption in 2SLS allowing for non-linear f in $Y = f(X) + U$, while still maintaining the additive noise assumption. By replacing both stages with kernel ridge regression they consistently estimate non-linear f in closed form.

3. *GB:* Kilbertus et al. (2020) further relax the additive noise assumption allowing for

---

[5]We remark that this work is focused on methods rather than novel biological insights. We do not claim robust biological insights for this specific dataset, as more scrutiny of the IV assumptions would be necessary. Even if valid, sub-therapeutic antibiotic treatment is a weak instrument in the real data, potentially causing bias in the IV estimates especially given the small sample size (Andrews et al., 2019).

general non-linear effects $Y = f(X, U)$. Under mild continuity assumptions for f, the causal effect is *partially* identifiable, and GB produces lower and upper bounds for $\mathbb{E}[Y | do(x)]$.

Figure 2 shows all three methods (including the naive single-stage OLS regression $X \rightarrow Y$) on the real data using Shannon diversity (left) and Simpson diversity (right) as the α-diversity measure. All three methods broadly agree for each diversity measure separately, supporting our confidence in the overall trends. However, we obtain *opposing* causal effects. While these opposing outcomes may not be unsettling given the differing diversity measures, they are still at odds with a single coherent notion of diversity as a meaningful causal driver of health outcomes.

To summarize, we have identified two main obstacles in using summary statistics for cause-effect estimation: (a) There is no consistent conceptualization of external interventions, mostly due to the 'many-to-one' nature, invalidating the intended causal conclusions. (b) We may observe opposing causal effects depending on the specific choice of summary statistic even when it is intended to carry the same semantic meaning. *Taken together, our findings challenge the common portrayal of summary statistics as a decisive (rather than merely descriptive) summary of compositions, and strongly advocate for causal effects to be estimated from the entire composition vector directly to establish a meaningful causal link between X and Y.*

4 Compositional causes

4.1 Methods for compositional causes

We now describe baseline methods as well as our proposals for estimating causal effects of compositions:

1. **2SLS.** As a baseline, we run 2SLS from eq. (2) directly on $X \in \mathbb{S}^{p-1}$ ignoring its compositional nature.

2. **2SLS$_{ILR}$.** 2SLS with ilr$(X) \in \mathbb{R}^{p-1}$ as the treatment; since OLS minima do not depend on the chosen basis, parameter estimates for different log-transformations of X are related via fixed linear transformations. Hence, as long as no sparsity penalty is added, ilr and alr regression yield equivalent results. The isometric ilr coordinates are useful due to the consistency guarantees of 2SLS given that $\mathbf{Z}^T$ ilr$(\mathbf{X})$ has full rank. However, for interpretability, moving to alr coordinates can be beneficial as components directly correspond to individual taxa (given a reference). The respective coordinate transformations are given in Appendix A.

3. **KIV$_{ILR}$.** Following Singh et al. (2019) we replace OLS in 2SLS$_{ILR}$ with kernel ridge regression in both stages to allow for non-linearities. Like 2SLS$_{ILR}$, KIV$_{ILR}$ cannot enforce sparsity in an interpretable fashion.

4. **ILR+LC.** To account for sparsity, we use sparse log-contrast estimation (see eq. (1)) for the second stage, while retaining OLS to ilr coordinates for the first stage.[6] Log-contrast estimation conserves interpretability in that the estimated parameters correspond directly to the effects of individual relative abundances.

5. **DIR+LC.** Finally, we circumvent log-transformations entirely and deploy regression methods that naturally work on compositional data in both stages. For the first stage,

---

[6]Since alr coordinates for X yield equivalent result in this method, we only report ILR+LC. All numbers match precisely for ALR+LC in our empirical evaluation.

we use a Dirichlet distribution—a common choice for modeling compositional data—where $X|Z \sim \text{Dirichlet}(\alpha_1(Z),\dots,\alpha_p(Z))$ with density $B(\alpha_1,\dots,\alpha_p)^{-1} \prod_{j=1}^{p} x_j^{\alpha_j-1}$ where we drop the dependence of $\alpha = (\alpha_1,\dots,\alpha_p) \in \mathbb{R}^p$ on Z for simplicity. With the mean of the Dirichlet distribution given by $\alpha/\sum_{j=1}^{p} \alpha_j$, we account for the Z-dependence via $\log(\alpha_j(Z_i)) = \omega_{0,j} + \omega_j^T Z_j$. We then estimate the newly introduced parameters $\omega_{0,j} \in \mathbb{R}$ and $\omega_j \in \mathbb{R}^q$ via maximum likelihood estimation with ℓ_1 regularization. For the second stage we again resort to sparse log-contrast estimation. There is room for discussion of the theoretical properties of this approach. If the non-linear first stage is misspecified, the "forbidden regression" bias may distort our effect estimates even in the limit of infinite data. We nevertheless include this method in our comparison, because the commonly used Dirichlet regression may result in a better fit of the data than linearly modeling log-transformations.

6. **Only LC.** For completeness we also run log-contrast estimation for the second stage only, ignoring the unobserved confounder.

4.2 Data generation

For the evaluation of our methods we require ground truth to be known. Since counterfactuals are never observed in practice, we simulate data (in two different settings) to maintain control over ground truth effects.

Setting A. The first setting is

$$Z_j \sim \text{Unif}(0,1), \qquad U \sim \mathcal{N}(\mu_c, 1), \tag{3}$$
$$\text{ilr}(X) = \alpha_0 + \alpha^T Z + U c_X, \qquad Y = \beta_0 + \beta^T \text{ilr}(X) + U c_Y,$$

where we model $\text{ilr}(X) \in \mathbb{R}^{p-1}$ directly and $\mu_c, c_Y \in \mathbb{R}$, $\alpha_0, c_X \in \mathbb{R}^{p-1}$, and $\alpha \in \mathbb{R}^{q \times (p-1)}$ are fixed up front. Our goal is to estimate the causal parameters $\beta \in \mathbb{R}^{p-1}$ and the intercept $\beta_0 \in \mathbb{R}$. This setting satisfies the standard 2SLS assumptions (linear, additive noise) and all our linear methods are thus *wellspecified*. To explore effects of *misspecification*, we also consider the same setting only replacing (using $\mathbf{1} = (1,\dots,1)$)

$$Y = \beta_0 + \frac{1}{10}\beta^T \text{ilr}(X) + \frac{1}{20}\mathbf{1}^T(\text{ilr}(X)+1)^3 + c_Y U. \tag{4}$$

Setting B. We now consider a sparse model for $X \in \mathbb{S}^{p-1}$ which is more realistic for higher-dimensional compositions. With $\mu = \alpha_0 + \alpha^T Z$ for fixed $\alpha_0 \in \mathbb{R}^p$ and $\alpha \in \mathbb{R}^{q \times p}$ we use[7]

$$Z_j \sim \text{Unif}(Z_{\min}, Z_{\max}), \qquad U \sim \text{Unif}(U_{\min}, U_{\max}),$$
$$X \sim C\big(\text{ZINB}(\mu, \Sigma, \theta, \eta)\big) \oplus (U \odot \Omega_C), \tag{5}$$
$$Y = \beta_0 + \beta^T \log(X) + c_Y^T \log(U \odot \Omega_C).$$

The treatment X is assumed to follow a zero-inflated negative binomial (ZINB) distribution (Greene, 1994), commonly used for modeling microbiome compositions (Xu et al., 2015). Here, $\eta \in (0,1)$ is the probability of zero entries, $\Sigma \in \mathbb{R}^{p \times p}$ is the covariance matrix, and $\theta \in \mathbb{R}$ the shape parameter. The confounder $U \in [U_{\min}, U_{\max}]$ perturbs this base composition in the direction of another fixed composition $\Omega_C \in \mathbb{S}^{p-1}$ scaled by U.[8] A linear combination of the log-transformed perturbation enters Y additively with weights $c_Y \in \mathbb{R}^p$ controlling

---

[7]Note that some variables have different dimensions in settings A and B.

[8]In simplex geometry $x_0 \oplus (U \odot x_1)$ corresponds to a line starting at x_0 and moving along x_1 by a fraction U.

Table 1: Results for setting A, which is fully linear in ilr(X), eq. (3).

Dimensions	Method	OOS MSE	β-MSE	FZ	FNZ
	DIR+LC	0.58 ±0.08	1.6 ±0.17	0.0	0.0
	ILR+LC[†]	**0.37** ±0.07	**1.1** ±0.15	0.0	0.0
$p = 3, q = 2$	KIV$_{\text{ILR}}$	**0.37** ±0.07	—	—	—
	Only LC	15.03 ±0.20	32.6 ±0.14	0.0	0.0
	2SLS	> 200	> 5k	0.0	0.0
	ILR+LC	**0.42** ±0.08	**0.22** ±0.01	0.0	0.04
$p = 30, q = 10$	KIV$_{\text{ILR}}$	257.9 ±34.3	—	—	—
	Only LC	24.4 ±0.37	1.90 ±0.00	0.0	0.0
	ILR+LC	**0.67** ±0.14	**0.22** ±0.02	0.0	0.0
$p = 250, q = 10$	KIV$_{\text{ILR}}$	5415.2 ±1127.6	—	—	—
	Only LC	30.8 ±0.48	143.3 ±0.27	3.0	1.0

[†] Identical to 2SLS$_{\text{ILR}}$ in low-dimensional setting without sparsity.

confounding strength. All other parameters choices are given in Appendix D. This setting is linear in how Z enters μ and how U enters X, Y in simplex geometry. All our two-stage models are (intentionally) misspecified in the first stage.

4.3 Metrics

Appropriate evaluation metrics are key for cause-effect estimation tasks. We aim at capturing the average causal effect (under interventions) and the causal parameters when warranted by modeling assumptions.

When the true effect is linear in $\log(X)$, we can compare the estimated causal parameters $\hat{\beta}$ from 2SLS$_{\text{ILR}}$, ILR+LC, and DIR+LC with the ground truth β directly. In these linear settings, we report causal effects of individual relative abundances X_j on the outcome Y via the mean squared difference (β-**MSE**) between the true and estimated parameters β and $\hat{\beta}$. Moreover, we also report the number of falsely predicted non-zero entries (**FNZ**) and falsely predicted zero entries (**FZ**), which are most informative in sparse settings.

In the general case, where a measure for identification of the interventional distribution $Y|do(X)$ is not straightforward to evaluate, we focus on the *out of sample error* (**OOS MSE**): For the true causal effect we first draw an i.i.d. sample $\{x_i\}_{i=1}^m$ from the data generating distribution (that are not in the training set, i.e., out of sample) and compute $\mathbb{E}_U[f(x_i, U)]$ for the known $f(X, U)$, the expected Y under intervention $do(x_i)$. We use $m = 250$ for all experiments. OOS MSE is then the mean square difference to our second-stage predictions $\hat{f}(x_i)$ on these out of sample x_i. Because in real observational data we do not have access to $Y|do(X)$ (but only $Y|X$), we need synthetic experiments.

4.4 Results

We run each method for 50 random seeds in setting A eq. (3) and for 20 random seeds in setting B eq. (5). We report mean and standard error over these runs. The sample size is $n = 1000$ in the low-dimensional case ($p = 3$) and $n = 10,000$ in the higher-dimensional cases ($p = 30$ and $p = 250$). For an in-depth sensitivity analysis of the main assumptions, we provide detailed explanations and results for misspecified and weak instrument scenarios in Appendix D and Appendix F.

Table 2: Results for setting B eq. (5), ZINB with sparse effects in higher dimensions for the first stage, where all our two-stage methods are (intentionally) misspecified in the first stage.

Dimensions	Method	OOS MSE	β-MSE	FZ	FNZ
$p = 3, q = 2$	DIR+LC	$> 10\text{k}$	$> 2\text{k}$	0.0	0.0
	ILR+LC[†]	**19.8** ±5.68	**10.2** ±4.44	0.0	0.0
	KIV$_{\text{ILR}}$	**18.9** ±5.23	—	—	—
	Only LC	277.7 ±8.43	131.1 ±2.29	0.0	0.0
	2SLS	$> 5\text{k}$	$> 100\text{k}$	0.0	0.0
$p = 30, q = 10$	ILR+LC	**99.0** ±9.89	**22.0** ±3.70	0.0	0.35
	KIV$_{\text{ILR}}$	283.5 ±25.0	—	—	—
	Only LC	3978.2 ±162.1	464.4 ±12.1	7.2	6.5
$p = 250, q = 10$	ILR+LC	**132.5** ±27.8	**42.7** ±14.5	0.05	0.55
	KIV$_{\text{ILR}}$	629.7 ±25.4	—	—	—
	Only LC	3417.8 ±157.0	511.8 ±15.2	6.8	2.1

[†] Identical to 2SLS$_{\text{ILR}}$ in low-dimensional setting without sparsity.

Low-dimensional experiments. We first consider settings A and B with $p = 3$ and $q = 2$. The top section of Table 1 and Table 2 show our metrics for all methods. First, we note that effect estimates are far off when ignoring the compositional nature (2SLS) or the confounding (Only LC).[9] Without sparsity in the second stage, 2SLS$_{\text{ILR}}$ and ILR+LC yield equivalent estimates in this low-dimensional linear setting—we only report ILR+LC. ILR+LC (and equivalent methods) succeed in cause-effect estimation under unobserved confounding: they recover the true causal parameters with high precision on average (low β-MSE) and thus achieve low OOS MSE. While DIR+LC performs reasonably well in setting A, setting B may surface a case of "forbidden regression" bias due to the misspecified first-stage. More detailed results and all remaining specifics of the simulation can be found in Appendix D and F.

Sparse high-dimensional experiments. We now consider the cases $p = 30$ and $p = 250$ with $q = 10$ and sparse ground truth β for setting A and setting B (8 non-zeros: 3 times $-5, 5$ and once $-10, 10$) in the bottom sections of Table 1 and Table 2. ILR+LC deals well with sparsity: unlike Only LC it identifies non-zero parameters perfectly (FZ=0) and rarely predicts false non-zeros. It also identifies true causal parameters and thus predicts interventional effects (OOS MSE) much better than Only LC. DIR+LC and 2SLS$_{\text{ILR}}$ fail entirely in these settings because the optimization does not converge. While we could get KIV$_{\text{ILR}}$ to return a solution, tuning the kernel hyperparameters for high-dimensional ilr coordinates becomes increasingly challenging, which is reflected in poor OOS MSE. Figure 3 shows box plots for the results in setting B to visualize the variation in the estimates across different runs. All simulation details and additional results are in Appendix D and F.

Real data. We return to the real data of (Schulfer et al., 2019). In Section 3, diversity is shown to lack causal explanatory power in general as well as explicitly for our dataset, see Figure 2. Naturally, ground truth is not available for real data. However, Figure 4 highlights that naive sparse log-contrast estimation proposes different influential microbes for the outcome than our two-stage ILR+LC. This indicates that the gut microbiome and body weight may indeed be confounded. Therefore, under the IV assumptions, the ILR+LC

---

[9]We note that recent non-linear IV methods such as Hartford et al. (2017); Bennett et al. (2019); Zhang et al. (2020) cannot overcome the issues of 2SLS in this setting.
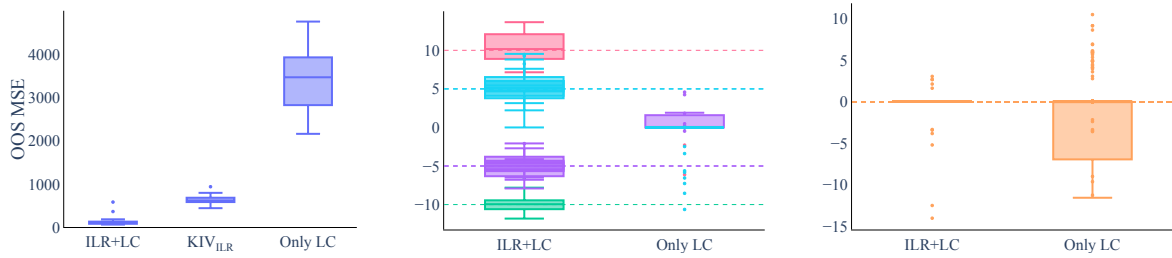
Figure 3: The boxplots below summarize the results for setting B in Table 2 with $p = 250, q = 10$. We collected the OOS MSE (left) as well as the non-zero β components (middle) and the zero β components (right). Only LC has troubles detecting non-zero components on average due to the lack of causal interpretation. All results and visualizations can be found in Appendix F.
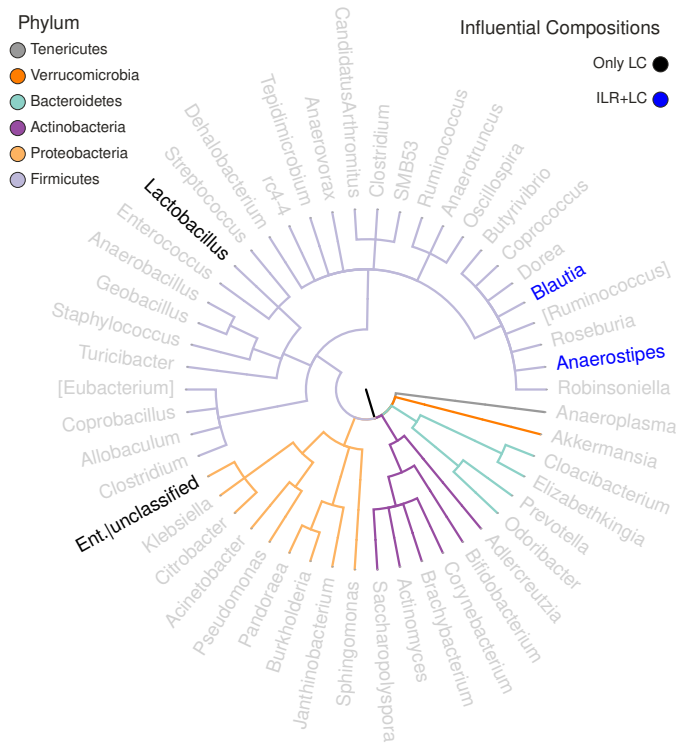

Figure 4: Taxonomic tree of the microbiome data at genus level. The influential log-ratios for both Only Second LC (black) and ILR+LC (blue) are disjoint.

estimates carry causal meaning for individual abundances, whereas direct log-contrast estimation solely surfaces correlation.

Discussion. Our results show that accounting for both the compositional nature as well as confounding is not optional for cause-effect estimation with compositional causes. Our two-stage methods not only reliably recover causal effects (OOS MSE), but also yield *interpretable* effect estimates for individual abundances (β-MSE, FZ, FNZ) whenever applicable. In particular, ILR+LC works reliably for non-sparse and sparse linear settings. When linearity cannot be assumed or interpretable estimates for individual components of β are not required, KIV_{ILR} can still perform well under these relaxed assumptions albeit being challenging to tune for large p and unable to incorporate sparsity. While DIR+LC in theory yields interpretable estimates and respects compositionality in both stages, our results highlight the danger of the "forbidden regression" with DIR+LC and we cannot recommend this seemingly superior method unless the data X are known to follow a Dirichlet distribution. ILR+LC appears to be largely unaffected by first stage misspecification.

5   Conclusion

The compositional nature of many scientific datasets poses major challenges to statistical analysis and interpretation—individual components are inherently entangled. Moreover, the analyst is often faced with a large number of possible components with the difficulty of identifying a parsimonious sub-composition of interest and has to deal with potential unobserved confounding. Given the potentially profound impact of the microbiome on human health or species abundances on global health, it is of vital importance that we face these challenges and develop interpretable methods to obtain causal insights from compositional data.

In this work, we developed and analyzed methods for cause-effect estimation with compositional causes under unobserved confounding in instrumental variable settings. As we aim for informing consequential decisions such as medical treatments, we focused on interpretability with respect to potential interventions. First, we crisply formulated the limitations of replacing compositions with information theoretic summary statistics using microbial diversity as a hall mark example.

Next, leveraging isometries to Euclidean space (e.g., ilr), we developed a range of methods for cause-effect estimation and provided an in-depth analysis of how IV assumptions (including misspecification or weak instrument bias) interact with compositionality. Neither can be ignored. We evaluated the efficacy and robustness of our methods in simulation and on real microbiome data. ILR+LC is particularly promising to provide interpretable and theoretically sound answers to causal queries involving compositional causes from purely observational data. Other seemingly well-suited methods such as DIR+LC fail, arguably due to an interaction of misspecification and the compositional nature of the data. We hope that we opened up avenues for future work on how to properly extend the causal inference toolbox to compositional causes as well as effects.

References

Aitchison, J. The statistical analysis of compositional data. *Journal of the Royal Statistical Society: Series B (Methodological)*, 44(2):139–160, 1982.

Aitchison, J. and Bacon-Shone, J. Log contrast models for experiments with mixtures. *Biometrika*, 71(2):323–330, 1984. ISSN 00063444. doi: 10.1093/biomet/71.2.323.

Andrews, I., Stock, J. H., and Sun, L. Weak instruments in instrumental variables regression: Theory and practice. *Annual Review of Economics*, 11:727–753, 2019.

Angrist, J. D. and Pischke, J.-S. *Mostly harmless econometrics: An empiricist's companion*. Princeton university press, 2008.

Arnold, K. F., Berrie, L., Tennant, P. W., and Gilthorpe, M. S. A causal inference perspective on the analysis of compositional data. *International journal of epidemiology*, 49(4):1307–1313, 2020.

Bello, M. G. D., Knight, R., Gilbert, J. A., and Blaser, M. J. Preserving microbial diversity. *Science*, 2018. ISSN 0036-8075. doi: 10.1126/science.aau8816.

Bennett, A., Kallus, N., and Schnabel, T. Deep generalized method of moments for instrumental variable analysis. In Wallach, H., Larochelle, H., Beygelzimer, A., d'Alché-Buc, F., Fox, E., and Garnett, R. (eds.), *Advances in Neural Information Processing Systems*, volume 32. Curran Associates, Inc., 2019. URL https://proceedings.neurips.cc/paper/2019/file/15d185eaa7c954e77f5343d941e25fbd-Paper.pdf.

Blaser, M. J. *Missing Microbes: How the Overuse of Antitbiotics Is Fueling Our Modern Plagues*. Henry Holt and Company, New York, first edit edition, 2014.

Blei, D. M. and Lafferty, J. D. Correlated topic models. *Advances in Neural Information Processing Systems*, pp. 147–154, 2005. ISSN 10495258.

Blei, D. M. and Lafferty, J. D. A correlated topic model of Science. *The Annals of Applied Statistics*, 1(1):17–35, 2007. ISSN 1932-6157. doi: 10.1214/07-aoas114.

Blundell, R., Chen, X., and Kristensen, D. Semi-nonparametric iv estimation of shape-invariant engel curves. *Econometrica*, 75(6):1613–1669, 2007.

Bonet, B. Instrumentality tests revisited. In *Proceedings of the 17th Conference on Uncertainty in Artificial Intelligence*, pp. 48–55, 2001.

Bradbury, J., Frostig, R., Hawkins, P., Johnson, M. J., Leary, C., Maclaurin, D., Necula, G., Paszke, A., VanderPlas, J., Wanderman-Milne, S., and Zhang, Q. JAX: Composable transformations of Python+NumPy programs, 2018.

Breskin, A. and Murray, E. J. Commentary: Compositional data call for complex interventions. *International Journal of Epidemiology*, 49(4):1314–1315, 2020.

Cammarota, G., Ianiro, G., Ahern, A., Carbone, C., Temko, A., Claesson, M. J., Gasbarrini, A., and Tortora, G. Gut microbiome, big data and machine learning to promote precision medicine for cancer. *Nature Reviews Gastroenterology and Hepatology*, 17(10):635–648, 2020. ISSN 17595053. doi: 10.1038/s41575-020-0327-3. URL http://dx.doi.org/10.1038/s41575-020-0327-3.

Chao, A., Chiu, C.-H., and Jost, L. Unifying species diversity, phylogenetic diversity, functional diversity, and related similarity and differentiation measures through hill numbers. *Annual review of ecology, evolution, and systematics*, 45:297–324, 2014.

Chapin, F. S., Zavaleta, E. S., Eviner, V. T., Naylor, R. L., Vitousek, P. M., Reynolds, H. L., Hooper, D. U., Lavorel, S., Sala, O. E., Hobbie, S. E., Mack, M. C., and Díaz, S. Consequences of changing biodiversity. *Nature*, 405(6783):234–242, 2000. ISSN 00280836. doi: 10.1038/35012241.

Cho, I. and Blaser, M. J. The human microbiome: at the interface of health and disease. *Nature Reviews Genetics*, 13(4):260–270, 2012.

Cho, I., Yamanishi, S., Cox, L., Methé, B. a., Zavadil, J., Li, K., Gao, Z., Mahana, D., Raju, K., Teitler, I., Li, H., Alekseyenko, A. V., and Blaser, M. J. Antibiotics in early life alter the murine colonic microbiome and adiposity. *Nature*, 488(7413):621–626, 2012. ISSN 0028-0836. doi: 10.1038/nature11400.

Clemente, J. C., Ursell, L. K., Parfrey, L. W., and Knight, R. The impact of the gut microbiota on human health: an integrative view. *Cell*, 148(6):1258–1270, 2012.

Combettes, P. and Müller, C. Regression models for compositional data: General log-contrast formulations, proximal optimization, and microbiome data applications. *Statistics in Biosciences*, 06 2020. doi: 10.1007/s12561-020-09283-2.

Daly, A. J., Baetens, J. M., and De Baets, B. Ecological diversity: measuring the unmeasurable. *Mathematics*, 6(7):119, 2018.

Egozcue, J. J., Pawlowsky-Glahn, V., Mateu-Figueras, G., and Barcelo-Vidal, C. Isometric logratio transformations for compositional data analysis. *Mathematical Geology*, 35(3):279–300, 2003.

Gautier, L., 2021. URL `https://rpy2.github.io/`.

Gloor, G. B., Macklaim, J. M., Pawlowsky-Glahn, V., and Egozcue, J. J. Microbiome datasets are compositional: and this is not optional. *Frontiers in microbiology*, 8:2224, 2017.

Greenacre, M. and Grunsky, E. The isometric logratio transformation in compositional data analysis: a practical evaluation. *preprint*, 2019. URL `https://ideas.repec.org/p/upf/upfgen/1627.html`.

Greene, W. H. Accounting for excess zeros and sample selection in poisson and negative binomial regression models. *NYU working paper no. EC-94-10*, 1994.

Gunsilius, F. Testability of instrument validity under continuous endogenous variables. *arXiv preprint arXiv:1806.09517*, 2018.

Harris, C. R., Millman, K. J., van der Walt, S. J., Gommers, R., Virtanen, P., Cournapeau, D., Wieser, E., Taylor, J., Berg, S., Smith, N. J., Kern, R., Picus, M., Hoyer, S., van Kerkwijk, M. H., Brett, M., Haldane, A., del Río, J. F., Wiebe, M., Peterson, P., Gérard-Marchant, P., Sheppard, K., Reddy, T., Weckesser, W., Abbasi, H., Gohlke, C., and Oliphant, T. E. Array programming with NumPy. *Nature*, 2020.

Hartford, J., Lewis, G., Leyton-Brown, K., and Taddy, M. Deep iv: A flexible approach for counterfactual prediction. In *International Conference on Machine Learning*, pp. 1414–1423, 2017.

Hernán, M. A. and Robins, J. M. Instruments for causal inference: an epidemiologist's dream? *Epidemiology*, pp. 360–372, 2006.

Hunter, J. D. Matplotlib: A 2D graphics environment. *Computing in Science & Engineering*, 2007.

Imbens, G. W. and Rubin, D. B. *Causal inference in statistics, social, and biomedical sciences*. Cambridge University Press, 2015.

Inc., P. T. Collaborative data science, 2015. URL `https://plot.ly`.

Kaul, A., Mandal, S., Davidov, O., and Peddada, S. D. Analysis of microbiome data in the presence of excess zeros. *Frontiers in microbiology*, 8:2114, 2017.

Kelejian, H. H. Two-stage least squares and econometric systems linear in parameters but nonlinear in the endogenous variables. *Journal of the American Statistical Association*, 66 (334):373–374, 1971.

Kilbertus, N., Kusner, M. J., and Silva, R. A class of algorithms for general instrumental variable models. In *Advances in Neural Information Processing Systems*, volume 33, 2020.

Kurtz, Z. D., Bonneau, R., and Müller, C. L. Disentangling microbial associations from hidden environmental and technical factors via latent graphical models. *bioRxiv*, 2019. doi: 10.1101/2019.12.21.885889.

Leinster, T. and Cobbold, C. Measuring diversity: The importance of species similarity. *Ecology*, 93:477–89, 03 2012. doi: 10.2307/23143936.

Lin, H. and Peddada, S. D. Analysis of microbial compositions: a review of normalization and differential abundance analysis. *NPJ biofilms and microbiomes*, 6(1):1–13, 2020.

Lin, W., Shi, P., Feng, R., and Li, H. Variable selection in regression with compositional covariates. *Biometrika*, 101(4):785–797, 2014. ISSN 14643510. doi: 10.1093/biomet/asu031.

Lynch, S. V. and Pedersen, O. The human intestinal microbiome in health and disease. *New England Journal of Medicine*, 375(24):2369–2379, 2016.

Mahana, D., Trent, C. M., Kurtz, Z. D., Bokulich, N. A., Battaglia, T., Chung, J., Müller, C. L., Li, H., Bonneau, R. A., and Blaser, M. J. Antibiotic perturbation of the murine gut microbiome enhances the adiposity, insulin resistance, and liver disease associated with high-fat diet. *Genome Medicine*, 8(1):1–20, 2016. ISSN 1756994X. doi: 10.1186/s13073-016-0297-9. URL `http://dx.doi.org/10.1186/s13073-016-0297-9`.

Muandet, K., Mehrjou, A., Lee, S. K., and Raj, A. Dual instrumental variable regression. *arXiv preprint arXiv:1910.12358*, 2019.

Newey, W. K. and Powell, J. L. Instrumental variable estimation of nonparametric models. *Econometrica*, 71(5):1565–1578, 2003.

Oh, M. and Zhang, L. Deepmicro: deep representation learning for disease prediction based on microbiome data. *Scientific Reports*, 10, 04 2020. doi: 10.1038/s41598-020-63159-5.

Oksanen, J., Blanchet, F. G., Friendly, M., Kindt, R., Legendre, P., McGlinn, D., Minchin, P. R., O'Hara, R. B., Simpson, G. L., Solymos, P., Stevens, M. H. H., Szoecs, E., and Wagner, H. *vegan: Community Ecology Package*, 2020. URL `https://CRAN.R-project.org/package=vegan`. R package version 2.5-7.

pandas development team, T. pandas-dev/pandas: Pandas, February 2020. URL `https://doi.org/10.5281/zenodo.3509134`.

Patuzzi, I., Baruzzo, G., Losasso, C., Ricci, A., and Di Camillo, B. metasparsim: a 16s rrna gene sequencing count data simulator. *BMC Bioinformatics*, 20, 11 2019. doi: 10.1186/s12859-019-2882-6.

Pawlowsky-Glahn, V. and Egozcue, J. J. Geometric approach to statistical analysis on the simplex. *Stochastic Environmental Research and Risk Assessment*, 15(5):384–398, 2001.

Pearl, J. On the testability of causal models with latent and instrumental variables. In *Proceedings of the Eleventh conference on Uncertainty in artificial intelligence*, pp. 435–443. Morgan Kaufmann Publishers Inc., 1995.

Pearl, J. *Causality*. Cambridge university press, 2009.

Pedregosa, F., Varoquaux, G., Gramfort, A., Michel, V., Thirion, B., Grisel, O., Blondel, M., Prettenhofer, P., Weiss, R., Dubourg, V., Vanderplas, J., Passos, A., Cournapeau, D., Brucher, M., Perrot, M., and Duchesnay, É. Scikit-learn: Machine learning in Python. *JMLR*, 2011.

Pflughoeft, K. J. and Versalovic, J. Human microbiome in health and disease. *Annual Review of Pathology: Mechanisms of Disease*, 7:99–122, 2012.

Quinn, T. P., Erb, I., Richardson, M. F., and Crowley, T. M. Understanding sequencing data as compositions: an outlook and review. *Bioinformatics*, 34(March):2870–2878, 2018. ISSN 1367-4803. doi: 10.1093/bioinformatics/bty175. URL `https://academic.oup.com/bioinformatics/advance-article/doi/10.1093/bioinformatics/bty175/4956011`.

Quinn, T. P., Nguyen, D., Rana, S., Gupta, S., and Venkatesh, S. DeepCoDA: personalized interpretability for compositional health data. *arXiv*, 2020.

R Core Team. *R: A Language and Environment for Statistical Computing*. R Foundation for Statistical Computing, Vienna, Austria, 2020. URL `https://www.R-project.org/`.

Rivera-Pinto, J., Egozcue, J. J., Pawlowsky-Glahn, V., Paredes, R., Noguera-Julian, M., and Calle, M. L. Balances: a new perspective for microbiome analysis. *MSystems*, 3(4):e00053–18, 2018.

Rozenblatt-Rosen, O., Stubbington, M. J., Regev, A., and Teichmann, S. A. The human cell atlas: from vision to reality. *Nature News*, 550(7677):451, 2017.

Rubin, D., Imbens, G., and Angrist, J. Identification of causal effects using instrumental variables: Rejoinder. *Journal of the American Statistical Association*, 91, 07 1993. doi: 10.2307/2291629.

Sanderson, E. and Windmeijer, F. A weak instrument f-test in linear iv models with multiple endogenous variables. *Journal of Econometrics*, 190(2):212–221, 2016. ISSN 0304-4076. doi: https://doi.org/10.1016/j.jeconom.2015.06.004. URL `https://www.sciencedirect.com/science/article/pii/S0304407615001736`. Endogeneity Problems in Econometrics.

Schulfer, A., Schluter, J., Zhang, Y., Brown, Q., Pathmasiri, W., McRitchie, S., Sumner, S., Li, H., Xavier, J., and Blaser, M. The impact of early-life sub-therapeutic antibiotic treatment (stat) on excessive weight is robust despite transfer of intestinal microbes. *The ISME Journal*, 13:1, 01 2019. doi: 10.1038/s41396-019-0349-4.

scikit-bio development team, T. scikit-bio: A bioinformatics library for data scientists, students, and developers, 2020. URL http://scikit-bio.org.

Seabold, S. and Perktold, J. statsmodels: Econometric and statistical modeling with python. In *9th Python in Science Conference*, 2010.

Sender, R., Fuchs, S., and Milo, R. Revised estimates for the number of human and bacteria cells in the body. *PLoS biology*, 14(8):e1002533, 2016.

Shade, A. Diversity is the question, not the answer. *The ISME journal*, 11(1):1–6, 2017.

Shreiner, A. B., Kao, J. Y., and Young, V. B. The gut microbiome in health and in disease. *Current opinion in gastroenterology*, 31(1):69, 2015.

Simpson, L., Combettes, P., and Müller, C. c-lasso - a python package for constrained sparse and robust regression and classification. *Journal of Open Source Software*, 6:2844, 01 2021. doi: 10.21105/joss.02844.

Singh, R., Sahani, M., and Gretton, A. Kernel instrumental variable regression. In *Advances in Neural Information Processing Systems*, pp. 4593–4605, 2019.

Sohn, M. B. and Li, H. Compositional mediation analysis for microbiome studies. *Annals of Applied Statistics*, 13(1):661–681, 2019. ISSN 19417330. doi: 10.1214/18-AOAS1210.

Suh, E. J., 2020. URL https://github.com/ericsuh/dirichlet.

Tsagris, M. and Athineou, G. *Compositional: Compositional Data Analysis*, 2021. URL https://CRAN.R-project.org/package=Compositional. R package version 4.5.

Turnbaugh, P. J., Ley, R. E., Hamady, M., Fraser-Liggett, C. M., Knight, R., and Gordon, J. I. The human microbiome project. *Nature*, 449(7164):804–810, 2007.

van Rossum, G. and Drake, F. L. *Python 3 Reference Manual*. CreateSpace, 2009.

Vujkovic-Cvijin, I., Sklar, J., Jiang, L., Natarajan, L., Knight, R., and Belkaid, Y. Host variables confound gut microbiota studies of human disease. *Nature 2020*, pp. 1–7, 2020. ISSN 0028-0836. doi: 10.1038/s41586-020-2881-9. URL http://www.nature.com/articles/s41586-020-2881-9{%}0Ahttps://www.nature.com/articles/s41586-020-2881-9?s=09.

Wang, C., Hu, J., Blaser, M. J., Li, H., and Birol, I. Estimating and testing the microbial causal mediation effect with high-dimensional and compositional microbiome data. *Bioinformatics*, 2020. ISSN 14602059. doi: 10.1093/bioinformatics/btz565.

Wes McKinney. Data Structures for Statistical Computing in Python. In Stéfan van der Walt and Jarrod Millman (eds.), *Proceedings of the 9th Python in Science Conference*, pp. 56 – 61, 2010. doi: 10.25080/Majora-92bf1922-00a.

Willis, A. Rarefaction, alpha diversity, and statistics. *Frontiers in Microbiology*, 10:2407, 10 2019. doi: 10.3389/fmicb.2019.02407.

Xu, L., Paterson, A. D., Turpin, W., and Xu, W. Assessment and selection of competing models for zero-inflated microbiome data. *PloS one*, 10(7):e0129606, 2015.

Zhang, R., Imaizumi, M., Schölkopf, B., and Muandet, K. Maximum moment restriction for instrumental variable regression. *arXiv preprint arXiv:2010.07684*, 2020.

A Compositional data transformations

Given a compositional vector $x \in \mathbb{S}^{p-1}$, the definitions of the log-transformations are given by the additive log-ratio transformation

$$\mathrm{alr}(x) := \left(\log \frac{x_1}{x_p}, \ldots, \log \frac{x_{p-1}}{x_p}\right) = \tilde{x}_{\mathrm{alr}} = \log(x) \cdot \begin{bmatrix} 1 & 0 & \cdots & 0 \\ 0 & 1 & \cdots & 0 \\ \vdots & \vdots & \ddots & \vdots \\ 0 & 0 & \cdots & 1 \\ -1 & -1 & \cdots & -1 \end{bmatrix} \tag{6}$$

with inverse

$$\mathrm{alr}^{-1}(\tilde{x}) = C(\exp([\tilde{x}, 0])), \tag{7}$$

the centered log-ratio transformation

$$\mathrm{clr}(x) := \left[\log \frac{x_1}{g(x)}, \ldots, \log \frac{x_p}{g(x)}\right] = \tilde{x}_{\mathrm{clr}} = \frac{\log(x)}{D} \cdot \begin{bmatrix} D-1 & -1 & \cdots & -1 \\ -1 & D-1 & \cdots & -1 \\ \vdots & \vdots & \ddots & \vdots \\ -1 & -1 & \cdots & D-1 \end{bmatrix} \tag{8}$$

with $g(x) := \sqrt[p]{x_1 \cdot \ldots \cdot x_p}$ and inverse

$$\mathrm{clr}^{-1}(\tilde{x}) = C(\exp([\tilde{x}])), \tag{9}$$

and the isometric log-ratio transformation

$$\mathrm{ilr}_V(x) = \tilde{x}_{\mathrm{ilr}} = \mathrm{clr}(x) \cdot V \tag{10}$$

for a matrix $V \in \mathbb{R}^{p \times p-1}$ such that $V^T V = \mathbb{I}_{p-1}$ providing an orthonormal basis of $\mathbb{R}^{p-1}$ with inverse

$$\mathrm{ilr}_V^{-1}(\tilde{x}) = C(\exp([\tilde{x} V^T])). \tag{11}$$

For the ilr transformation, a typical choice for V^T is the so-called Helmert matrix with the first row removed (see for example `http://scikit-bio.org/docs/0.4.1/generated/generated/skbio.stats.composition.ilr.html`).

B Instrumental variable methods

We consider three different approaches that gradually relax some of the common IV assumptions. In particular, the restrictions on the function space of f are gradually relaxed in the different settings.

The Two Stage Least Squares algorithm (2SLS) consists of two sequential OLS regressions (Rubin et al., 1993). 2SLS is one of the most prominent approaches. It allows for unobserved confounding while still putting linear restrictions on the function space of f and assuming additive noise:

$$Y = \beta X + \epsilon_Y \tag{12}$$

First, 2SLS fits a regression model based on Z to predict X. The second stage uses the estimated $\hat{X}$ to predict Y. This results in the following estimator for β:

$$\hat{\beta} = \left(X^T P_Z X\right)^{-1}\left(X^T P_Z y\right) \tag{13}$$

with $P_Z = Z(Z^T Z)^{-1} Z^T$.

If $p = q$, the estimator reduces to the following form:

$$\hat{\beta} = \left(Z^T X\right)^{-1}\left(Z^T y\right) \tag{14}$$

Singh et al. (2019) relax the assumption of the linear setting in 2SLS towards a non-parametric generalization of the causal effect by applying kernel ridge regression (KIV).

$$Y = f(X) + \epsilon_Y, \tag{15}$$

for a potentially non-linear f, maintaining the additive noise assumption for point-identifiability.

The OLS regressions are replaced by kernel ridge regressions and thus model the relationship of Z, X and Y by non-linear functions in reproducing kernel Hilbert spaces (RKHSs). This method still requires additive noise models to produce consistent results. Following the arguments in Singh et al. (2019), this gives us a closed form solution for f:

$$W = K_{XX}(K_{ZZ} + n\lambda Id)^{-1} K_{Z\tilde{Z}} \tag{16}$$

$$\hat{\alpha} = (WW^T + m\xi K_{XX})^{-1} W\tilde{y}, \tag{17}$$

$$\hat{f}_\xi^m(x) = (\hat{\alpha})^T K_{Xx} \tag{18}$$

In the next step, we drop the assumption of additive noise, i.e., allowing $f(X, U)$ to depend on the treatment X and any (potentially high-dimensional) confounder U in arbitrary ways (also non-linearly). This implies that the effect is only partially identifiable, i.e., we can only put lower and upper bounds on $\mathbb{E}[Y|do(x)]$. Kilbertus et al. (2020) employ the response function framework to minimize (maximize) the average causal effect over all causal models that satisfy the structural IV assumptions and simultaneously match the observed data to find the lower (upper) bound. We refer the reader to the original paper for the details (Kilbertus et al., 2020).

C Package references

Here, we briefly outline the software used in our empirical evaluation. Please note that the code and the requirements are all available at `https://github.com/EAiler/comp-iv`.

C.1 Python packages

We use the following Python (van Rossum & Drake, 2009) packages: Plotly (Inc., 2015), Numpy (Harris et al., 2020), Scipy (Wes McKinney, 2010), scikit-learn (Pedregosa et al., 2011), scikit-bio (scikit-bio development team, 2020), rpy2 (Gautier, 2021), Matplotlib (Hunter, 2007), Statsmodels (Seabold & Perktold, 2010), Pandas (pandas development team, 2020), Jax (Bradbury et al., 2018), Dirichlet (Suh, 2020), c-Lasso (Simpson et al., 2021).

C.2 R packages

We use the following R (R Core Team, 2020) packages: SpiecEasi (Kurtz et al., 2019), vegan (Oksanen et al., 2020), Compositional (Tsagris & Athineou, 2021) and metaSparSim (Patuzzi et al., 2019).

D Data generation

This section describes the details of how we generate data for our empirical evaluation. Complementary to the real microbiome data, we consider several approaches to generate data for the compositional instrumental variable setting. Since counterfactuals are never observed in practice, we need a setup where the ground truth is known and can be controlled. We choose to simulate data from two different data generating models, Setting A and Setting B. The first one will put (most of) our models in a wellspecified setting, where we have strong expectations and theoretical guarantees on how they will behave. The other approach simulates compositional data by a zero-inflated negative binomial. Thus, the first stage of all of our models will be misspecified (except for potentially KIV assuming a proper choice of the kernels). This allows us to test our models for robustness and probe their limitations.

Based on this motivation, we also describe two additional parameter settings within Setting A that will examine robustness and limitations: a weak instrument scenario and a scenario with a non-linear second stage f. The first scenario will test the necessity of a strong/valid instrument, the second scenario will further look into the issue of misspecification (now in the second stage).

We describe the data generating model and the specific parameter settings. We also provide visualizations of the resulting data distributions, which is rather tricky for compositional data with $p > 3$. We will then supplement the result section of the main text with additional comments on the evaluation of the results and show the complete set of plots for Table 1 and Table 2.

Each generated dataset for $p = 3$ comprises $n = 1000$ samples, resp. 10,000 samples for $p = 30$ and $p = 250$, with an additional $n_{\text{intervention}} = 250$ interventional samples for evaluation of OOS MSE. Note that the examples in the figures show only one of these datasets. To ensure reproducibility, we consistently chose the 10th dataset of the confidence runs for (a representative) visualization.

D.1 Setting A

The following explanations refer to *Setting A* described in section 4.2 in the main part.

Setting A generates data that enables us to assess our methods in a *wellspecified* setting. Instead of modeling $X \in \mathbb{S}^{p-1}$ directly, we model ilr(X). The setting is strictly linear in ilr(X). This means that both g and f are linear functions of U and Z, resp., U and ilr(X). The generative model is as follows:

$$
\begin{aligned}
Z_j &\sim \text{Uniform}(0,1) \\
U &\sim \mathcal{N}(\mu_c, 1) \\
\text{ilr}(X) = g(Z, U) &= \alpha_0 + \alpha Z + c_X U \\
Y = f(X, U) &= \beta_0 + \beta^T \text{ilr}(X) + c_Y U
\end{aligned}
\tag{19}
$$

D.1.1 Setting A with $p = 3, q = 2$

The main characteristics of this lower dimensional dataset are the presence of all microbes and relatively seldom zero values. We choose the following parameters for the low-dimensional case:

$$
\mu_c = -3, \alpha_0 = [1,1], \alpha = \begin{bmatrix} 0.5 & -0.15 \\ 0.3 & 0.7 \end{bmatrix}, c_X = [0.5, 0.5], \beta_0 = 0.5, \beta = [4,1], c_Y = 4
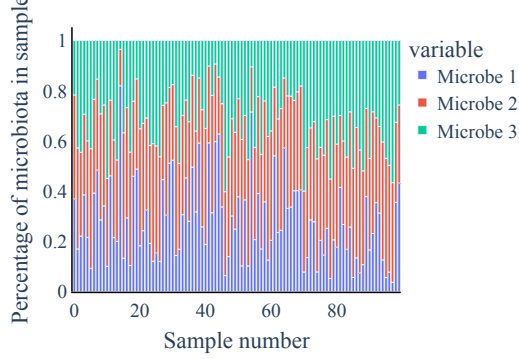$$

Figure 5: **Setting A with** $p = 3$, $q = 2$: The barplot shows the three-part composition of the first 100 samples. The microbes are evenly distributed over the individual compositions.
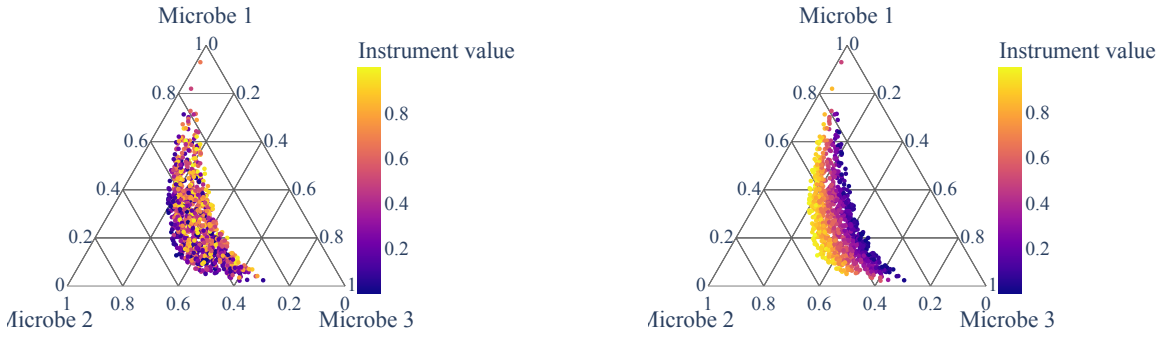

Figure 6: **Setting A with** $p = 3$, $q = 2$: The ternary plots are colored by first (left) and second (right) instrument value. The influence of Z_2 on the composition X is particularly pronounced and visually supports the assumption of Z being a valid instrument.

The first stage F-test for the two components of $\text{ilr}(X)$ gives $(32.18, 113.99)$ for the 10th data sample.[10]

For the $p = 3$ case, we can visualize X by its compositional coordinates not only in a barplot (Figure 5) but also in an arguably more informative ternary plot (Figure 6). To visualize the linear relationship between observed $\text{ilr}(X)$ and Y as well as the true effect $Y|do(X)$, we transform the data X and visualize each component in a separate scatter plot (see Figure 7).

D.1.2   Setting A with $p = 30, q = 10$

Contrary to the previous example, we now analyze a slightly higher-dimensional setting with $p = 30$. In this scenario, it makes sense to introduce sparsity in the data generation process from a practical viewpoint. We work with the data generation setting given in eq. (19) and
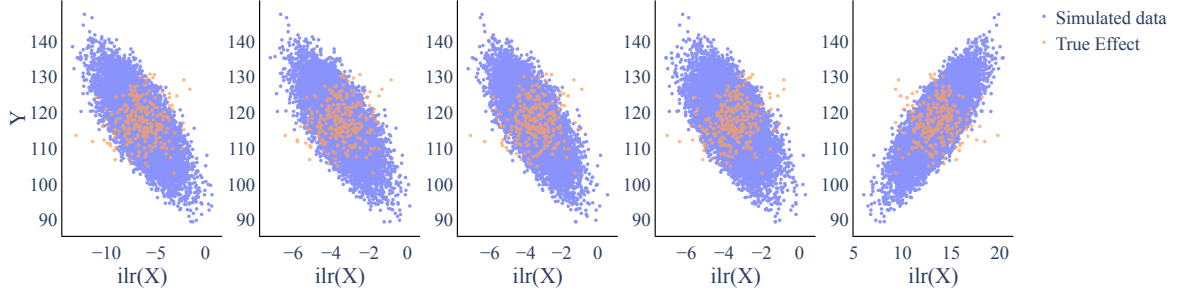
---

[10]We remark that in higher dimensions, the F-test does not provide a strong theoretical justification for sufficient instrument strength, but we still use it as a sensible heuristic that provides a relative measure between different settings, i.e., in which scenario the instrument is stronger.
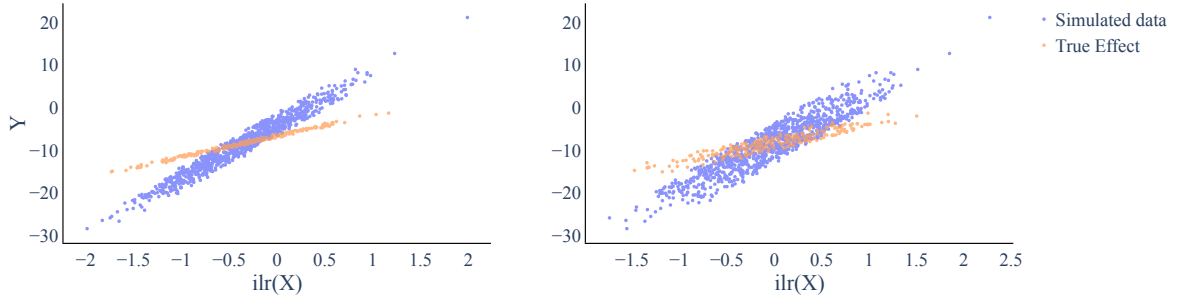
Figure 7: **Setting A with $p = 3$, $q = 2$:** Both plots show one component of $\text{ilr}(X) \in \mathbb{R}^2$ vs. the confounded outcome (blue) and the true effect (orange). Due to the confounding, the observed and the causal effect do not overlap. However, we expect the instrument Z to factor out the confounding effect and enable the two stage methods to identify the causal effect.
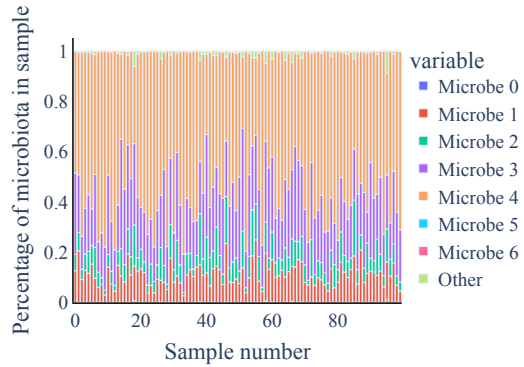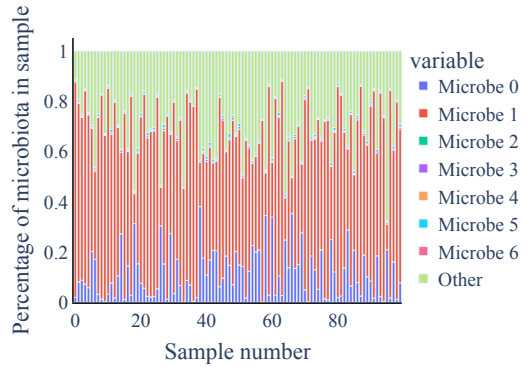

Figure 8: **Setting A with $p = 30$, $q = 10$:** The barplot shows the composition of the first 100 samples. The compositions are dominated by a few species.

choose the following parameters:

$$\mu_c = 5, \alpha_0 = [3,1,1,1,3,1,1,1,0,\cdots,0], \alpha_{ij} \begin{cases} 0, & \text{for } i \neq j \text{ and } i,j > 8, \\ 1, & \text{for } i \neq j \leq 8 \end{cases},$$

$$c_X = [-2,-1,-1,-1,2,1,1,1,0,\cdots,0], \beta_0 = 5, \beta_{\log} = [10,5,5,5,-10,-5,-5,-5,0,\cdots,0],$$

$$\beta = V^T \cdot \beta_{\log}, c_Y = 5$$

for $i \in \{1,\ldots,p-1\}, j \in \{1,\ldots,q\}$ and V providing the orthonormal basis for the ilr-transformation (see Appendix A).

Since a visualization with a ternary plot is no longer feasible, we only show barplots of the data in Figure 8. However, scatter plots showing individual $\text{ilr}(X)$ coordinates versus the observed Y and the true causal effect are still informative. Since the first components are the most influential ones in our setting, we show the first five $\text{ilr}(X)$ components in Figure 9.

D.1.3 Setting A with $p = 250, q = 10$

We now analyze the second high-dimensional setting with $p = 250$. As in the scenario of $p = 30$, it makes sense to introduce sparsity in the data generation process from a practical viewpoint. We work with the data generation setting given in eq. (19) and choose the
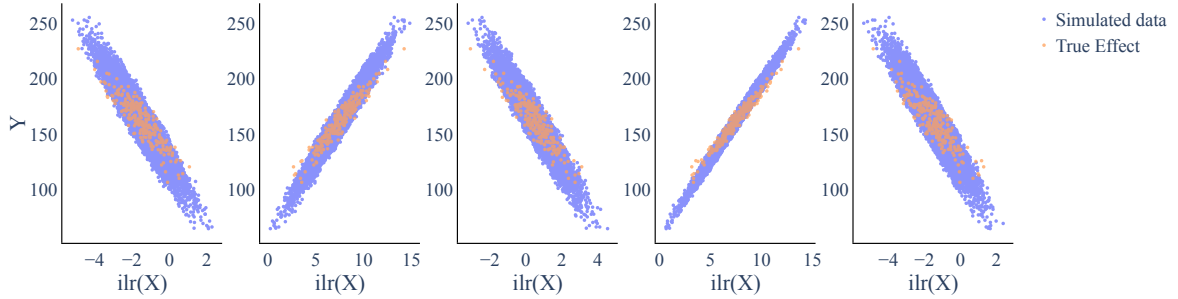
23

Figure 9: **Setting A with** $p = 30$, $q = 10$ **:** Both plots show one component of ilr$(X) \in \mathbb{R}^{29}$ vs. the confounded outcome (blue) and the true effect (orange). Due to the confounding, the observed and the causal effect do not overlap. However, we expect the instrument Z to factor out the confounding effect and enable the two stage methods to identify the causal effect.

Figure 10: **Setting A with** $p = 250$, $q = 10$**:** The barplot shows the composition of the first 100 samples. The compositions are dominated by a few species.

following parameters:

$$\mu_c = 3, \; \alpha_0 = [1,1,3,1,1,1,3,1,1,1,3,1,0,\cdots,0], \; \alpha_{ij} \begin{cases} 0, & \text{for } i \neq j \text{ and } i,j > 8, \\ 1, & \text{for } i \neq j \leq 8 \end{cases},$$

$$c_X = [-1,2,-1,2,-1,2,-2,1,-2,1,-2,1,0,\cdots,0], \; \beta_0 = 5, \; \beta_{\log} = [10,5,5,5,-10,-5,-5,-5,0,\cdots,0],$$

$$\beta = V^T \cdot \beta_{\log}, \; c_Y = 5$$

for $i \in \{1,\dots,p-1\}, j \in \{1,\dots,q\}$ and V providing the orthonormal basis for the ilr-transformation (see Appendix A). Since a visualization with a ternary plot is no longer feasible, we only show barplots of the data in Figure 10. However, scatter plots showing individual ilr(X) coordinates versus the observed Y and the true causal effect are still informative. Since the first components are the most influential ones in our setting, we show the first five ilr(X) components in Figure 11.

D.2   Setting B

The following explanations refer to *Setting B* described in section 4.2 in the main part.

Setting B serves three main purposes: (i) to assess our methods on a dataset that closely resembles real-world data in terms of its distribution, (ii) to assess our methods when the first stage is misspecified, and (iii) to allow for sparsity in the first stage of the data generating process, resembling the real data in Schulfer et al. (2019). The sparsity of the

Figure 11: **Setting A with** $p = 250, q = 10$**:** Both plots show one component of $\mathrm{ilr}(X) \in \mathbb{R}^{249}$ vs. the confounded outcome (blue) and the true effect (orange). Due to the confounding, the observed and the causal effect do not overlap. However, we expect the instrument Z to factor out the confounding effect and enable the two stage methods to identify the causal effect.

compositional data can be accomplished by a zero-inflated negative binomial distribution. As ZINegBinomial is a frequently used distribution in modeling microbiome data, we assume a closer resemblance to real world sparsity than the resemblance we achieve in Setting A for $p = 30$ and $p = 250$.

The data is generated according to the following model with the parameter μ of the negative binomial as $\mu = \alpha_0 + \alpha Z$:

$$
\begin{aligned}
Z_j &\sim \mathrm{Uniform}(Z_{\min}, Z_{\max}), \\
U &\sim \mathrm{Uniform}(U_{\min}, U_{\max}), \\
X = g(Z, U) &\sim C(\mathrm{ZINegBinomial}(\mu, \Sigma, \theta, \eta)) \oplus (\Omega_C \odot U), \\
Y = f(X, U) &= \beta_0 + \beta^T \log(X) + c_Y^T \log(\Omega_C \odot U)
\end{aligned}
\tag{20}
$$

We fix $Z_{\min} = 1, Z_{\max} = 10$ and $U_{\min} = 0.2, U_{\max} = 3$ throughout. For the negative binomial distribution we set $\Sigma = \mathbb{I}_p$, i.e., assuming no additional correlation within the different components of the composition for simplicity.

D.2.1 Setting B with $p = 3, q = 2$

The parameter setting with $p = 3$ does not yet contain sparse data due to its low-dimensionality. It serves the purpose to compare the performance of the two stage methods in a misspecified setting and a wellspecified setting (except for DIR+LC which is misspecified in both Setting A and Setting B).

Here, we consider the following generative model based on eq. (20). We fix $Z_{\min} = 0, Z_{\max} = 10, U_{\min} = 0.2, U_{\max} = 3$. We chose α_0 to be $[7, 9, 8]$ and $\alpha = \begin{bmatrix} 5 & 0 & 0 \\ 0 & 5 & 0 \\ 0 & 0 & 5 \end{bmatrix}$ to guarantee for valid instruments. We set the dispersion to $\theta = 2$ and keep the zero probability at $\eta = [0, 0, 0]$ to get valid compositions for this low-dimensional scenario. For the confounding composition Ω_C, we set it to $[0.7, 0.1, 0.2]$. For the second stage, we fix ground truth parameters $\beta_0 = 1, \beta_{\log} = [-5, 3, 2]$, which results in $\beta = V^T \beta_{\log}$ and the confounding parameter $c_Y = [2, -10, -10]$.

The first stage F-test for the two components of $\mathrm{ilr}(X)$ gives $(41.38, 14.08)$ for the 10th data sample.[11]

---

[11]We remark that in higher dimensions, the F-test does not provide a strong theoretical justification for
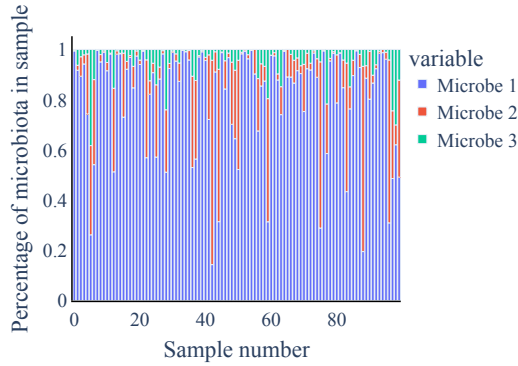
Figure 12: **Setting B with $p = 3$, $q = 2$:** The barplot shows the three-part composition of the first 100 samples. The data sample shows some dominating species in the individual compositions while having more variation between the samples compared to Setting A.
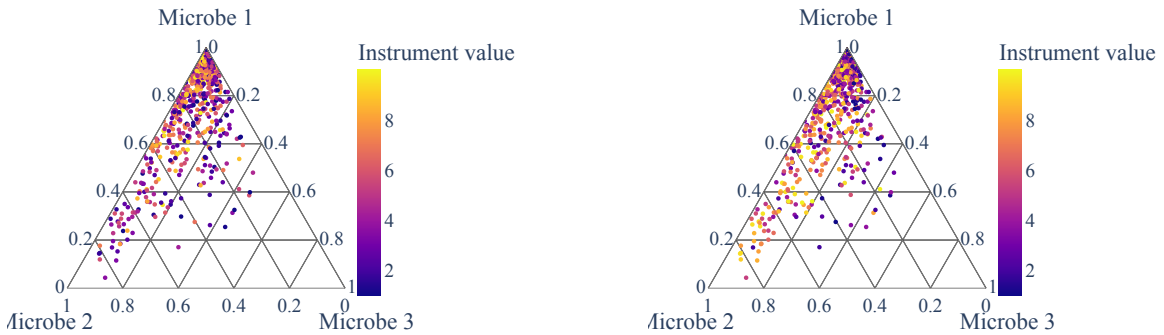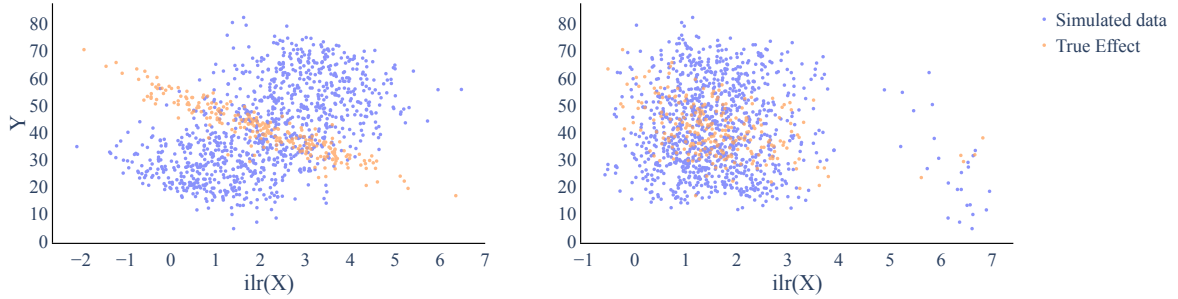

Figure 13: **Setting B with $p = 3$, $q = 2$:** The ternary plots are colored by first (left) and second (right) instrument value. Due to the data generation process, the influence of Z_1 and Z_2 on the composition X is less visually obvious than for Setting A. Nevertheless, Z can be assumed to be a valid instrument.

For the $p = 3$ case, we can visualize X by its compositional coordinates not only in a barplot (Figure 12) but also in an arguably more informative ternary plot (Figure 13). To visualize the relationship between observed $\mathrm{ilr}(X)$ and Y as well as the true effect $Y|do(X)$, we transform the data X and visualize each component in a separate scatter plot (see Figure 14).

D.2.2   Setting B with $p = 30, q = 10$

In the higher-dimensional scenarios we will make us of the sparsity ability of the ZINegBinom distribution.

The parameters were chosen to generate a suitable dataset that still conveys typical compositional data properties (sparsity, high variance within the composition, similar means to real data) and significant instruments. Here, we consider the following generative model based on eq. (20). We fix $Z_{\min} = 0, Z_{\max} = 10, U_{\min} = 0.2, U_{\max} = 3$. To ensure a handful of components dominating the composition, we fix the first 8 entries of α_0 to be $[1, 1, 2, 1, 4, 4, 2, 1, 4, 4, 2, 1]$ and randomly sample the remaining ones from $\mathrm{UniformChoice}([1, 2, 2])$. For α, which mainly controls the instrument strength, we use a deterministic value to guarantee valid

---

sufficient instrument strength, but we still use it as a sensible heuristic that provides a relative measure between different settings, i.e., in which scenario the instrument is stronger.

Figure 14: **Setting B with** $p = 3$, $q = 2$: Both plots show one component of $\mathrm{ilr}(X) \in \mathbb{R}^2$ vs. the confounded outcome (blue) and the true effect (orange). Due to the confounding, the observed and the causal effect do not overlap. However, we expect the instrument Z to factor out the confounding effect and enable the two stage methods to identify the causal effect.
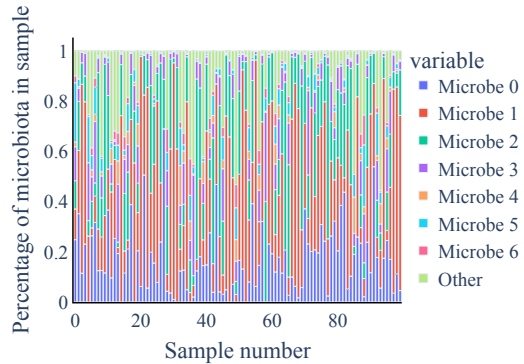

Figure 15: **Setting B with** $p = 30$, $q = 10$: The barplot shows the different compositions of the first 100 samples in the dataset. We observe some dominating components and many small components with an overall high variability.

instruments:

$$\alpha_{ij} \begin{cases} 0, & \text{for } i \neq j \text{ and } i, j > 8, \\ 1, & \text{for } i \neq j \leq 8 \end{cases}$$

We set the dispersion to $\theta = 2$ and the zero probability value $\eta = [0, \dots, 0, 0.8, \dots, 0.8]$. For the confounding composition Ω_C, we fix the first components to $[0.2, 0.3, 0.2, 0.1]$, to ensure that the most dominating parts of the composition are also more strongly influenced by confounding. Then we sample the remaining components of Ω_C from UniformChoice$([0.01, 0.05])$ and eventually apply the closure operator C to ensure Ω_C is a composition. For the second stage, we fix ground truth parameters $\beta_0 = 1$, $\beta_{\log} = [-10, -5, -5, -5, 10, 5, 5, 5, 0, \dots, 0]$, which results in $\beta = V^T \beta_{\log}$ and the confounding parameter $c_Y = [10, 10, 5, 15, -5, -5, -5, -5, -5, -5, -5, -5, 0, \dots, 0]$.

For a brief overview, we visualize the first five components of the $\mathrm{ilr}(X)$ coordinates versus the observed Y and the true causal effect in Figure 16 and show barplots of the generated data in Figure 15.

D.2.3 Setting B with $p = 250, q = 10$

We consider now the second high-dimensional scenario for Setting B with $p = 250$. The parameters for Setting B with $p = 250$ are very close to the parameters for Setting B with $p = 30$.
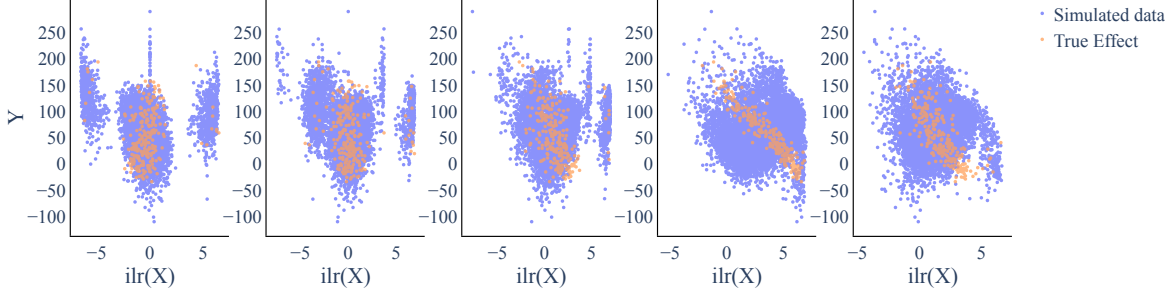
Figure 16: **Setting B with** $p = 30$, $q = 10$: Each plot shows one of the first five components of $\mathrm{ilr}(X) \in \mathbb{R}^{29}$ vs. the confounded outcome (blue) and the true effect (orange). The dataset shows strong confounding in some of the components as the true effect and the observed effect actually contradict each other. We expect the two stage methods to perform better than the naive regression in such scenarios. We can thus check if the two stage methods are still able to make use of the instrument Z despite the misspecified first stage.

Again, we consider the following generative model based on eq. (20). We fix $Z_{\min} = 0, Z_{\max} = 10, U_{\min} = 0.2, U_{\max} = 3$. To ensure a handful of components dominating the composition, we fix the first 8 entries of α_0 to be $[1, 1, 2, 1, 4, 4, 2, 1, 4, 4, 2, 1]$ and randomly sample the remaining ones from UniformChoice($[1, 2, 2]$). For α, which mainly controls the instrument strength, we use a deterministic value to guarantee valid instruments:

$$\alpha_{ij} \begin{cases} 0, & \text{for } i \neq j \text{ and } i, j > 8, \\ 1, & \text{for } i \neq j \leq 8 \end{cases}$$

We set the dispersion to $\theta = 2$ and the zero probability value $\eta = [0, \dots, 0, 0.8, \dots, 0.8]$. For the confounding composition Ω_C, we fix the first components to $[0.2, 0.3, 0.2, 0.1]$, to ensure that the most dominating parts of the composition are also more strongly influenced by confounding. Then we sample the remaining components of Ω_C from UniformChoice($[0.01, 0.05]$) and eventually apply the closure operator C to ensure Ω_C is a composition. For the second stage, we fix ground truth parameters $\beta_0 = 1$, $\beta_{\log} = [-10, -5, -5, -5, 10, 5, 5, 5, 0, \dots, 0]$, which results in $\beta = V^T \beta_{\log}$ and the confounding parameter $c_Y = [10, 10, 5, 15, -5, -5, -5, -5, -5, -5, -5, -5, 0, \dots, 0]$.

For a brief overview, we visualize the first five components of the $\mathrm{ilr}(X)$ coordinates versus the observed Y and the true causal effect in Figure 18 and show barplots of the generated data in Figure 17.

D.3 Further settings for robustness estimation

By assuming a misspecified first stage in Setting B via the ZINegBinom distribution, we already started to evaluate the robustness of our methods. Nevertheless, we will further relax different requirements within Setting A. We evaluate the robustness via two additional scenarios

1. We relax the assumption of a valid instrument and test the sensitivity of the methods with respect to weak instruments.

2. We assume a non-linear ground truth relationship f for the second stage, a scenario for which all the considered models are misspecified.
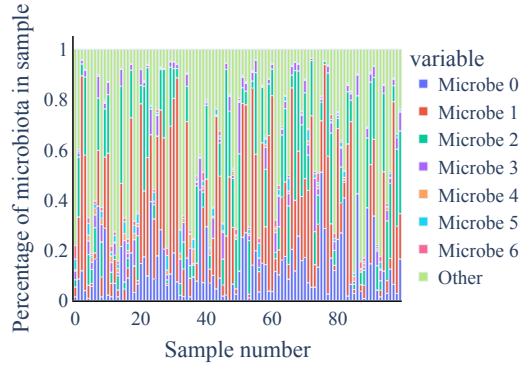
28

Figure 17: **Setting B with** $p = 250$, $q = 10$**:** The barplot shows the different compositions of the first 100 samples in the dataset. We still observe a few dominating components and many small components with an overall high variability.
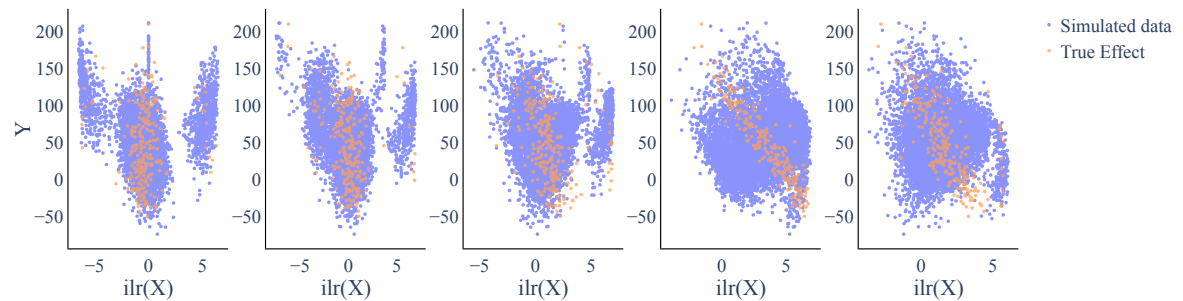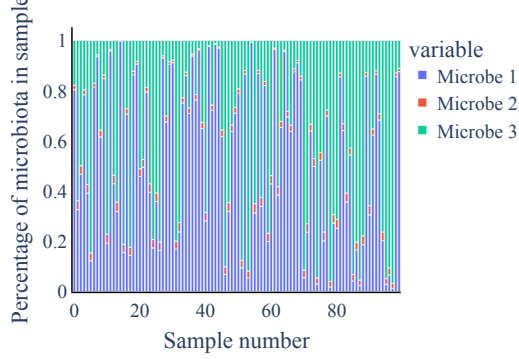

Figure 18: **Setting B with** $p = 250$, $q = 10$**:** Each plot shows one of the first five components of ilr$(X) \in \mathbb{R}^{249}$ vs. the confounded outcome (blue) and the true effect (orange). The dataset shows strong confounding in some of the components as the true effect and the observed effect actually contradict each other. We expect the two stage methods to perform better than the naive regression in such scenarios. We can thus check if the two stage methods are still able to make use of the instrument Z despite the misspecified first stage.

Figure 19: **Setting A with** $q = 2$, $p = 3$ **and weak instruments:** The barplot shows the different composition in each sample (plotted here for the first 100 samples). Microbe 2 has a relatively small value whereas microbe 1 and microbe 3 dominate the composition by high variation.

D.3.1 Weak instrument(s)

"Strong instruments" resp. "valid instruments" are a prerequisite for successful two-stage estimation and one of the key discussion points in applications of two-stage instrumental variable estimation. Instrument strength for $p = 1$ is typically measured via the first-stage F-statistic with a value >10 being considered sufficient to avoid weak instrument bias in 2SLS (Andrews et al., 2019). For $p > 1$, measuring instrument strength is not as straightforward (Sanderson & Windmeijer, 2016) and we thus report F-statistics for each dimension of the treatment (either $X \in \mathbb{S}^{p-1}$ or $\mathrm{ilr}(X) \in \mathbb{R}^{p-1}$) separately. Theoretically, the estimation bias can become arbitrarily large (even in the large data limit) for weak instruments. To quantitatively assess the effect of weak instruments in our specific applications, we provide an additional simulation scenario and its results (see Appendix F) for a weak instrument settings.

Setting A with $p = 3$, $q = 2$ **and weak instruments**   For testing in a weak instrument setting, we return to Setting A. We mostly control the instrument strength via α and use higher or lower α values to obtain a strong or weak instrument setting. We choose the following parameters for a weak instrument:

$$\mu_c = -2, \alpha_0 = [4, 1], \alpha = \begin{bmatrix} 0.15 & 0.15 \\ 0.2 & 0 \end{bmatrix}, c_X = [1, 1], \beta_0 = 2, \beta = [6, 2], c_Y = 4$$

The first stage F-test for the two components of $\mathrm{ilr}(X)$ gives $(4.84, 1.77)$, much weaker than the previous settings. Again we show a barplot (Figure 19) and a ternary plot (Figure 20) of the generated data. The observed data as well as the true causal effect are shown in Figure 21.

D.3.2 Nonlinear second stage

Contrary to the previous scenarios, we now consider a non-linear f, resulting in a misspecified second stage for most of our methods. Note that in this scenario all two-stage methods as well as the naive regression will be misspecified in the second stage.

Setting A with $p = 3$, $q = 2$ **and non-linear** f Specifically, we replace the linear function for Y in eq. (19) with

$$Y = \beta_0 + \frac{1}{10}\beta^T \mathrm{ilr}(X) + \frac{1}{20}\mathbf{1}^T (\mathrm{ilr}(X) + 1)^3 + c_Y U. \tag{21}$$
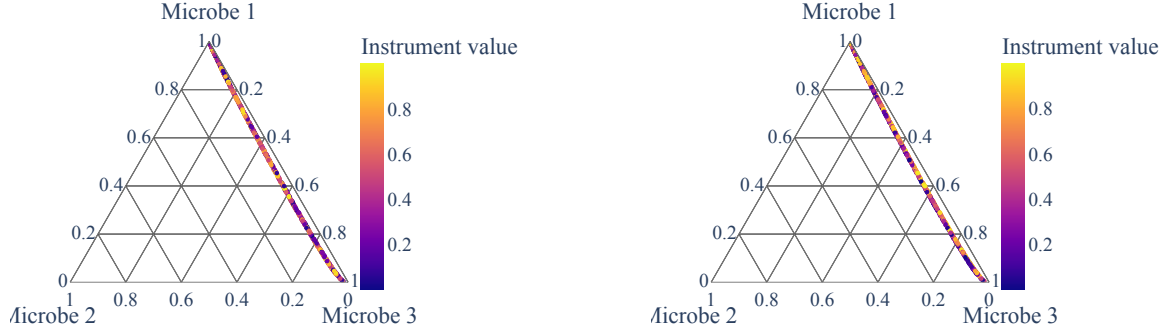
Figure 20: **Setting A with** $q = 2$**,** $p = 3$ **and weak instruments:** The ternary plots are colored by first (left) and second (right) instrument. The composition of the instrument is barely influenced by the value of Z.
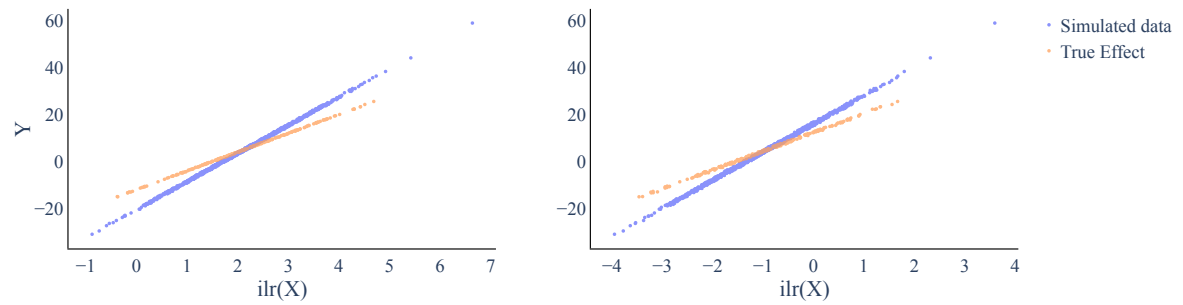

Figure 21: **Setting A with** $q = 2$**,** $p = 3$ **and weak instruments:** Both plots show one component of ilr(X) $\in \mathbb{R}^2$ vs. the confounded outcome (blue) and the true effect (orange). Due to the confounding, both effects do not overlap. As we are in the weaker instrument setting, we expect the methods to perform not as stable as in the previous cases where we had a stronger instrument available.
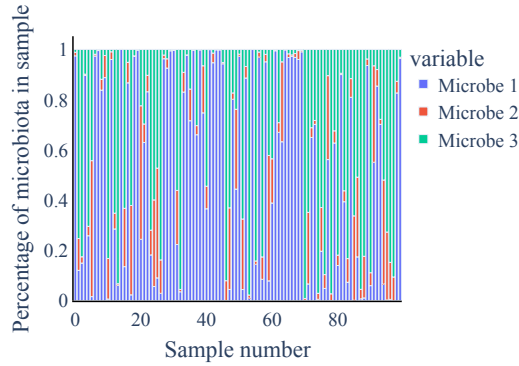
Figure 22: **Setting A with $p = 3$, $q = 2$ and a non-linear function form of f:** The barplot shows the different composition for each sample (for the 100 first data points). Microbe 1 and 2 dominate the composition with high variance.
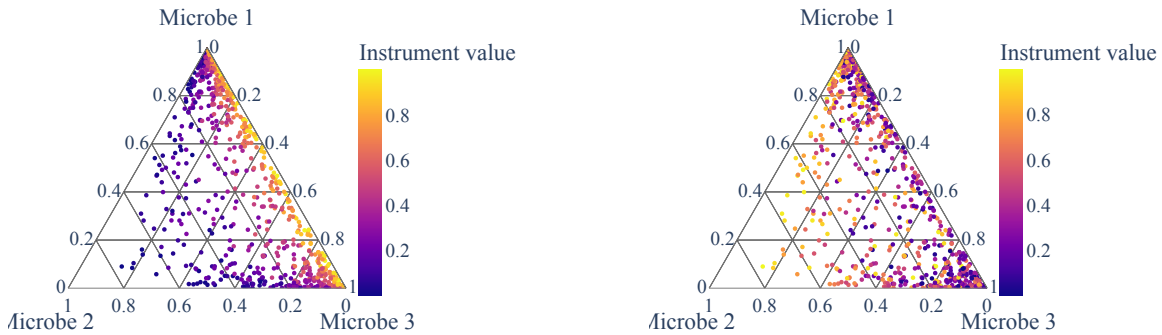
Figure 23: **Setting A with $p = 3$, $q = 2$ and a non-linear function form of f:** The ternary plots for the non-linear setup with $q = 2$, colored by first (left) and second (right) instrument. Note that the first stage is still linear in $\mathrm{ilr}(X)$. Thus, the generation of the X values is not affected by the change in f.

The remaining parameters are chosen to yield a strong instrument, ensuring that any performance differences are not (in addition) due to weak instrument bias:

$$\mu_c = -1, \alpha_0 = [1, 1], \alpha = \begin{bmatrix} 4 & 1 \\ -1 & 3 \end{bmatrix}, c_X = [2, 2], \beta_0 = 0.5, \beta = [6, 2], c_Y = 4$$

Note that in this setting β cannot be interpreted directly as the causal parameters, since the true causal effect also has a non-linear dependence on $\mathrm{ilr}(X)$. Since the first stage remains unchanged, we can still use an F-test to assess instrument strength, which results in $(164.7, 133.3)$, a solid indicator for a strong instrument. Again we show a barplot (Figure 22) and a ternary plot (Figure 23) of the generated data. The observed data as well as the true causal effect are shown in Figure 24.
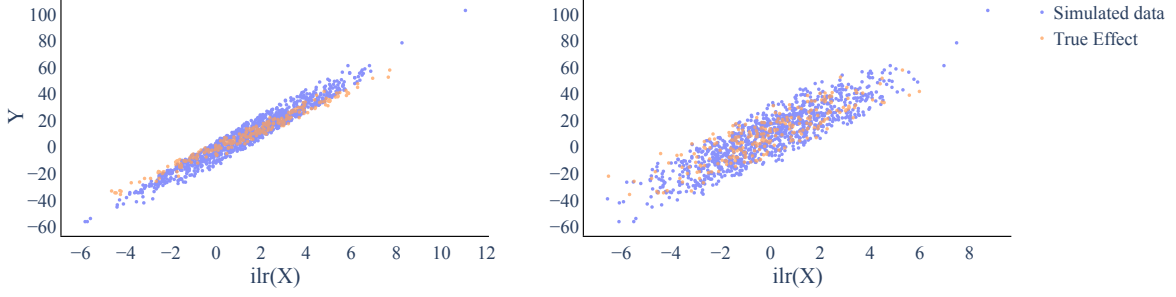
Figure 24: **Setting A with $p = 3$, $q = 2$ and a non-linear function form of f:** Both plots show one component of $\mathrm{ilr}(X) \in \mathbb{R}^2$ vs. the confounded outcome (blue) and the true effect (orange). The effect both of the confounded outcome and the true effect show a non-linear dependency towards the individual $\mathrm{ilr}(X)$ components.

E   Method training

E.1   Dirichlet regression

The mean of the Dirichlet distribution is given by $\mu_{\mathrm{Diri}} = \frac{\alpha_j}{\sum_{j=1}^{p} \alpha_j}$. Here, we consider the following model for the mean components

$$\mathbb{E}[X_{ij}] = \frac{\alpha_j}{\sum_{j=1}^{p} \alpha_j} = \frac{\alpha_j(Z_i)}{\sum_{j=1}^{p} \alpha_j(Z_i)} \tag{22}$$

$$\log(\alpha_j(Z_i)) = \omega_{0j} + \omega_j Z_j. \tag{23}$$

The maximum likelihood function is then given by

$$l(\alpha; X, Z) = \frac{1}{n} \sum_{i=1}^{n} \log \Gamma \left(\sum_{j=1}^{p} \exp\{\omega_{0j} + \omega_j Z_i\} \right) \tag{24}$$

$$+ \frac{1}{n} \sum_{i=1}^{n} \sum_{j=1}^{p} \left(\log(X_{ij}) \left(\exp\{\omega_{0j} + \omega_j Z_i\} - 1 \right) - \log \Gamma \left(\exp\{\omega_{0j} + \omega_j Z_i\} \right) \right). \tag{25}$$

Additionally, we introduce a sparsity enforcing regularization term to arrive at the following objective function

$$\min_{\omega} -l(\alpha; X, Z) + \lambda_{\mathrm{dirichlet}} \sum_{j=1}^{p} |\omega_j| \tag{26}$$

with $\lambda_{\mathrm{dirichlet}} \geq 0$. For each Dirichlet regression, we pick $\lambda_{\mathrm{dirichlet}}$ from the set $\{0.1, 1, 2, 5, 10\}$ by model selection via the Bayesian Information Criterion ($BIC = q \cdot \log(n) - 2 \cdot (\hat{L})$, with $\hat{L}$ being the likelihood value). We train the model for each available λ value in the set and choose the model with minimal BIC. For the starting point α_{start} we fit a Dirichlet distribution on those X for which all $|Z| < 0.2$ by maximum likelihood estimation.

E.2   Log-contrast regression

The log-contrast regression is enforcing sparsity via an ℓ_1 penalty on the β parameters.

$$\min_{\beta} \sum_{i=1}^{n} \mathcal{L}(x_i, y_i, \beta) + \lambda \|\beta\|_1 \quad \text{s.t.} \sum_{i=1}^{p} \beta_i = 0. \tag{27}$$

This estimation respects the compositional nature of x while retaining the association between the entry β_i and the relative abundance of the individual taxon x_i.

In our examples, we focus mainly on continuous $y \in \mathbb{R}$ and the squared loss $\mathcal{L}(x, y, \beta) = (y - \beta^T \log(x))^2$. However, the framework in Section 4 also supports different loss functions.

For robust Lasso regression, the Huber loss can be applied.

$$\mathcal{L}(x_i, y_i, \beta) = \mathcal{H}_\delta(x_i, y_i, \beta) = \begin{cases} \frac{1}{2}(y_i - \beta^T \log(x_i))^2 & \text{for } |y_i - \beta^T \log(x_i)| < \delta \\ \delta(|y_i - \beta^T \log(x_i)| - \frac{1}{2}\delta), & \text{otherwise.} \end{cases} \tag{28}$$

The Huber Loss combines the squared loss and the absolute loss. It is less sensitive to outliers than the squared loss, but remains differentiable at 0 in contrast to the absolute loss.

Moreover, for classification tasks with $y_i \in \{-1, 1\}$, we can directly use the squared Hinge loss for $\mathcal{L}$ with:

$$\mathcal{L}(x_i, y_i, \beta) = l(x_i, y_i, \beta) \text{ with } l(x_i, y_i, \beta) = \begin{cases} (1 - (y_i \beta^T \log(x_i))^2, & \text{if } y_i \beta^T \log(x_i) \leq 1 \\ 0, & \text{if } y_i \beta^T \log(x_i) > 1 \end{cases} \tag{29}$$

or a "Huberized" version thereof:

$$\mathcal{L}(x_i, y_i, \beta) = l_\delta(x_i, y_i, \beta) \text{ with } l_\delta(x_i, y_i, \beta) = \begin{cases} (1 - (y_i \beta^T \log(x_i))^2, & \text{if } \delta \leq y_i \beta^T \log(x_i) \leq 1 \\ (1 - \delta)(1 + \delta - 2y_i \beta^T \log(x_i)), & \text{if } y_i \beta^T \log(x_i) \leq \delta \\ 0, & \text{if } y_i \beta^T \log(x_i) > 1 \end{cases} \tag{30}$$

We refer to Simpson et al. (2021) for further loss functions and a more detailed overview.

We now continue with the description of the setup used in the following result section. The results on the synthetic data and the real data in Appendix F are based on the squared loss:

$$\min_\beta \sum_{i=1}^n \|y_i - \beta^T \log(x_i)\|_2^2 + \lambda \|\beta\|_1 \quad \text{subject to} \sum_{i=1}^p \beta_i = 0.$$

Furthermore, for the real data we also show the results for a binary outcome $y_i \in \{-1, 1\}$ based on the squared Hinge loss (eq. 29).

We solve the underlying optimization problems with the c-lasso package, a Python package for constrained sparse regression (Simpson et al., 2021). The c-lasso packages comprises several model selection schemes, including a theoretically-derived λ_0 parameter, k-fold cross-validation, and stability selection.

Here, we consider stability selection for tuning λ. The method comprises the hyperparameter $t_{\text{threshold}}$ which determines the number of coefficients included in the final model. In our training, we set the same $t_{\text{threshold}}$ for the naive regression as well as the two stage methods to have a fair comparison. In all our training scenarios with generated data we find $t_{\text{threshold}} = 0.7$ to be a reasonable default value. For the real data scenario we found $t_{\text{threshold}} = 0.65$ to be more sensible.

We use Setting B with $p = 30$ and $q = 10$ as a representative example to illustrate the impact of the threshold value. Figure 25 shows the stability profile of the β coefficients and their attributed probability of entering the model. The threshold value $t_{\text{threshold}} = 0.7$ works as a cut off for the relevant coefficients. The upper panel shows the results for the naive regression, whereas the lower panel shows the results for the ILR+LC regression (working on the exact same data).
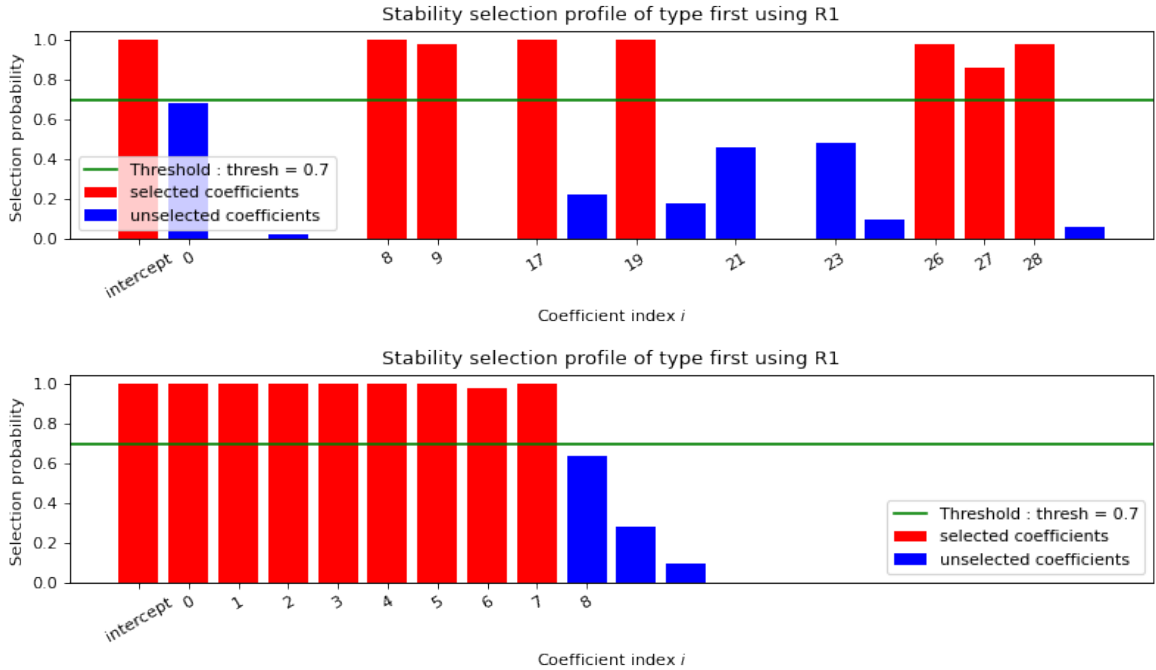
Figure 25: **Stability profiles for sparse log contrast regression with c-lasso:** The barplots show the model selection probability of the β coefficients. The upper panel shows the example for the naive regression. The lower panel shows the results for the same setting for ILR+LC regression. Both models are fairly certain about the main drivers.

Moreover, the method also returns the coefficient values across the λ-path, i.e., the entry of coefficients into the model for the corresponding λ (see Figure 26). Further improvements may be achieved by taking the path and individual analysis into account instead of proposing a general $t_{\text{threshold}}$, however, this simple yet effective approach was sufficient for our purposes in this work.

F   Additional results

For the comparison of the different methods, we make use of three approaches:

1. $\hat{\beta}$-MSE: As long as the second stage is wellspecified and linear, we can compare the estimated causal parameters $\hat{\beta}$ for the various approaches (where applicable).

2. *FZ/FNZ*: As long as the second stage is wellspecified and linear, we can additionally compare the number of false zero values and false non-zero values to quantify support recovery.

3. *OOS MSE*: In the general case, the causal performance measure is measured by an "out of sample error"(*OOS MSE*) which denotes the mean squared error between the true value of Y under an intervention $do(X = x)$ and the predicted causal effect $\mathbb{E}[Y|do(X)]$ of our model, given by $\hat{f}(x)$. For the interventional X, we simulate 250 additional compositional data points according to the underlying model, but using a different seed and thus disconnecting them from the instrument Z and the confounder U. Thus, we receive a true interventional X which still preserves data characteristics.

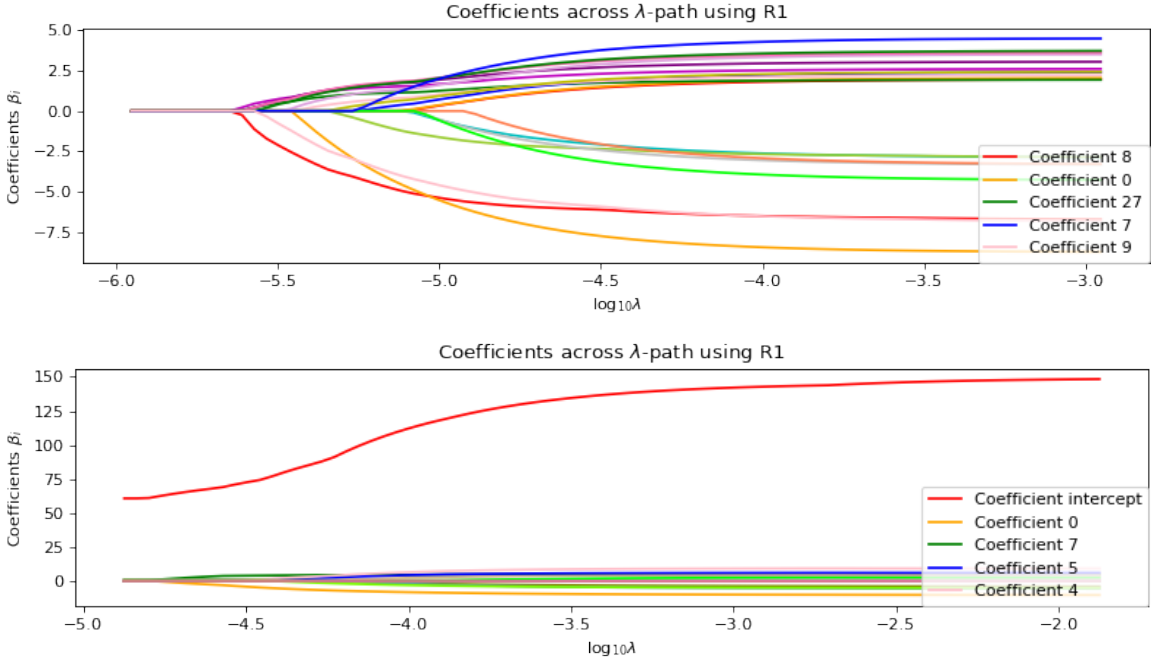For each data generating setup, we provide confidence intervals for the methods' results by

Figure 26: **Corresponding λ-path for β coefficients:** The plots show the individual coefficients for the different λ values. The upper plot shows the β coefficients for the naive regression, the lower plot presents the coefficients for the two stage method ILR+LC.

performing the data generation and the method evaluation 50 times on different random seeds. In each run, we sample $n = 1000$ datapoints in the $p = 3$ scenario and 10,000 datapoints in the $p = 30$ and $p = 250$ scenario. We compute the OOS MSE as well as the $\hat{\beta}$-MSE and FZ/FNZ (if applicable). Some of the figures in this section are extended or more complete versions of the numbers given in the table in the main body (see Table 1 and Table 2), where some less relevant results have been omitted for readability.

F.1 Setting A

F.1.1 Setting A with $p = 3, q = 2$

This setting is a wellspecified setting for ALR+LC, 2SLS$_{\text{ILR}}$ and ILR+LC. Moreover, confounding is present (see Figure 7) which additionally gives us reason to expect a much better performance of the two stage methods than the naive regression $X \rightarrow Y$ in terms of OOS MSE. The results in Figure 27, largely verify this expectation. The naive regression has a clear disadvantage due to confounding and picks up on spurious correlations as an effect coming from X. Two stage methods work well when relying on a strong instrument, helping the methods to factor out the confounding and identifying the true casual effect. Figure 28 shows the causal parameter estimates $\hat{\beta}$ and further corroborates our claims that two-stage methods significantly outperform naive regression. The effects found via naive regression overestimate the direct causal effect strength from X, whereas all two stage methods recover the true causal parameters β well. Only DIR+LC suffers slightly from the misspecified first stage compared to the other wellspecified two stage approaches. It is noteworthy that DIR+LC works reasonably well despite our manual two stage procedure with a "forbidden" non-linear regression in the first stage. Since we are in the low-dimensional setting with no sparsity regularization, the results of ILR+LC, ALR+LC and 2SLS$_{\text{ILR}}$ are equivalent.
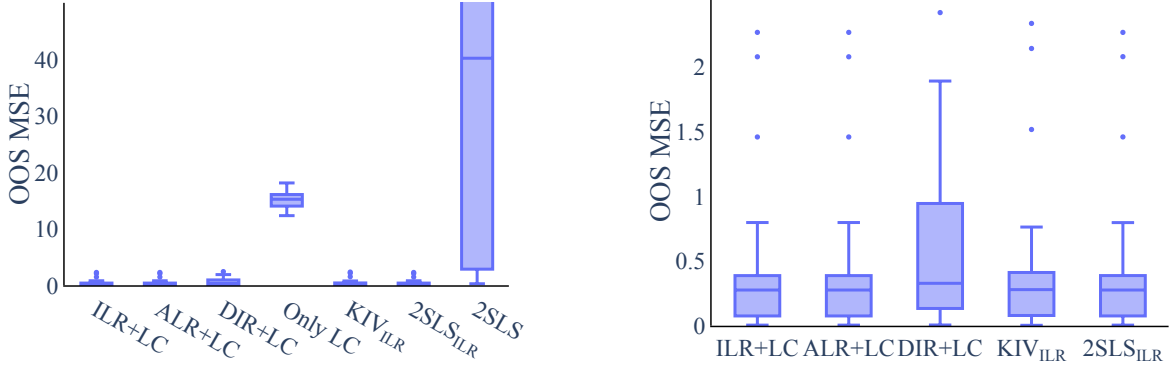
36

Figure 27: **Setting A with** $p = 3$, $q = 2$: The boxplots show the OOS MSE of 50 runs. The naive regression Only LC and 2SLS (left) perform way worse compared to the other approaches. When we adjust the y-scale (right), DIR+LC also shows a higher OOS MSE than ILR+LC etc. DIR+LC possibly suffers from the misspecified first stage. Note that ALR+LC,ILR+LC, $2SLS_{ILR}$ are equivalent in the low-dimensional case.
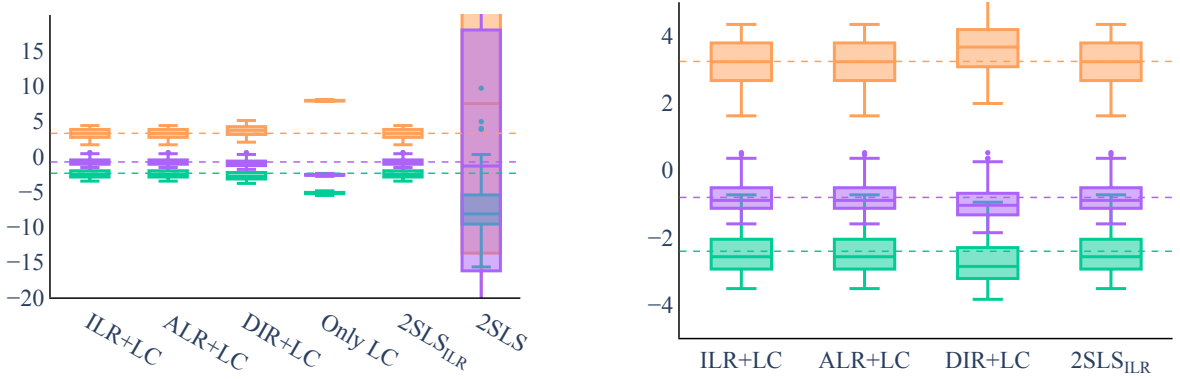

Figure 28: **Setting A with** $p = 3$, $q = 2$: The boxplots show the $\hat{\beta}$ values for the 50 runs for each of the 3 β coefficients (dashed lines). The two stage methods, except 2SLS, are able to recover the causal effect on average. The naive regression method overestimates the effect. Moreover, it does so with a high degree of confidence as there is barely any variation in the $\hat{\beta}$ estimates (left). When we adjust the y-scale (right), DIR+LC shows a notable bias towards the solution of the naive regression (left). This might suggest that DIR+LC indeed suffers from the misspecified first stage and thus is not able to make use of the instrument Z as efficiently.
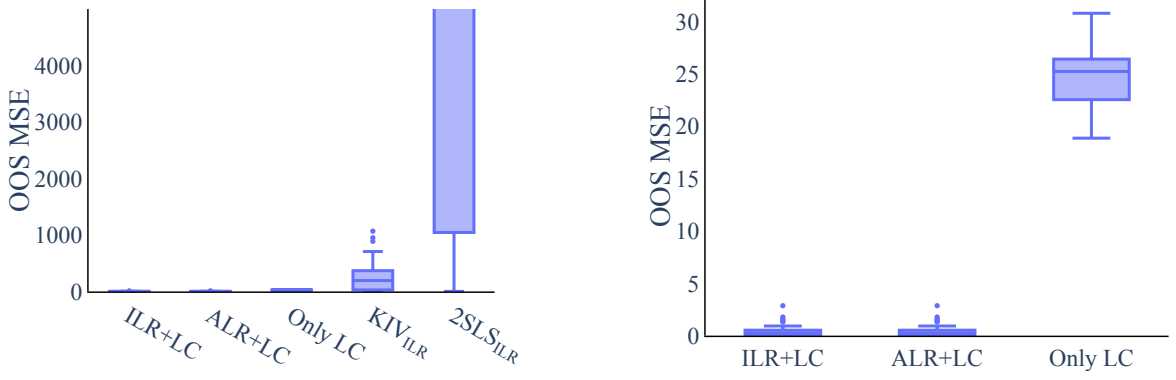
Figure 29: **Setting A with** $p = 30$**,** $q = 10$**:** The boxplots show the OOS MSE of 50 runs. 2SLS_{ILR} and KIV_{ILR} are volatile and lack sensible regularization (left). When we adjust the y-scale, we see that Only LC (right) performs also way worse compared to the regularized two stage approaches.

F.1.2 Setting A with $p = 30, q = 10$

Microbiome compositional data is typically high-dimensional and comprises many zero values. Moreover, it is often assumed that only a few microbial compositions (and hence β parameters) influence an outcome of interest Y. Thus, in the following, we aim to be close to such a scenario by assuming a sparse β as ground truth and by simulating X with a few dominating compositions in the data generating process (see Appendix D).

Note that for higher-dimensional approaches, we omit results for DIR+LC due to computational issues stemming from the maximum likelihood estimation of the α_0 and α parameters in the first stage. 2SLS, which ignores the compositionality of X altogether, is not able to converge at all.

For higher dimensions, the lack of regularization in the ILR methods becomes obvious (Figure 29), both for 2SLS_{ILR} and KIV_{ILR}. The methods become more volatile and 2SLS_{ILR} is unable to detect any zero values in β (see Figure 30). On the other hand, the naive regression is able to identify zero βs correctly, but suffers from confounding and thus over- or underestimates the true influential βs. Only the regularized two stage approaches are able to recover the true causal βs, both the influential coefficients as well as the zero values.

F.1.3 Setting A with $p = 250, q = 10$

To further test the approaches, we use another high-dimensional setup with $p = 250$. Again, we make use of the common assumption that only a few microbial compositions (and hence β parameters) influence an outcome of interest Y. We assume a sparse β as ground truth and run the models on X which has a few dominating species.

Note that for higher-dimensional approaches, we omit results for DIR+LC due to computational issues stemming from the maximum likelihood estimation of the α_0 and α parameters in the first stage. 2SLS, which ignores the compositionality of X altogether, is not able to converge at all.

For $p = 250$, the problem of missing regularization in the ILR methods (2SLS_{ILR} and KIV_{ILR}) becomes even more pronounced (Figure 31). For readability we thus omitted 2SLS_{ILR} from the β plots. Moreover, the naive regression is not even able to recover the full support, as it
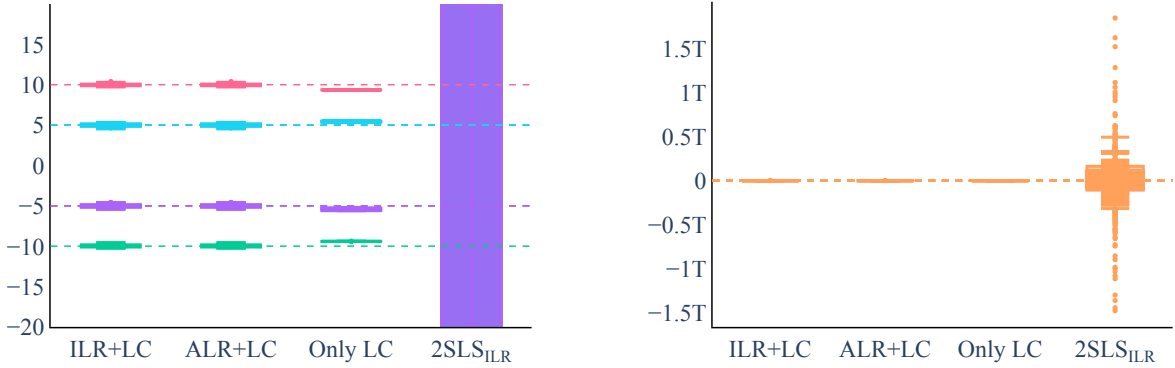
Figure 30: **Setting A with** $p = 30$, $q = 10$: The boxplots show the $\hat{\beta}$ values for the 50 runs for each of the 8 non-zero β coefficients (dashed lines, left) and the 22 zero β coefficients (dashed line, right). The two stage methods are able to recover the causal effect on average, whereas the naive regression methods overestimate the effect (left). Moreover, Only LC does so with a high degree of confidence as there is barely any variation in the $\hat{\beta}$ estimates. $2SLS_{ILR}$ does not produce sensible estimates due to the missing regularization.
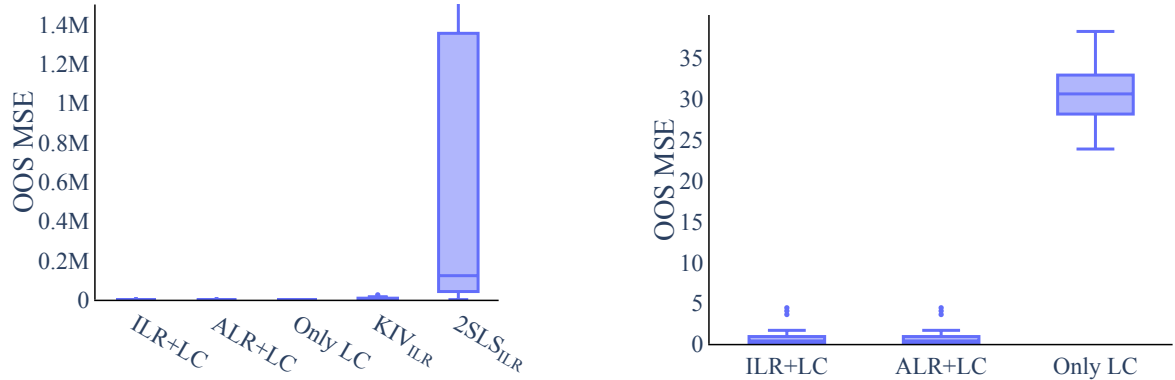
Figure 31: **Setting A with** $p = 250$, $q = 10$: The boxplots show the OOS MSE of 50 runs. $2SLS_{ILR}$ and KIV_{ILR} are volatile and lack sensible regularization (left). This problem is more pressing as the dimensionality grows. When we adjust the y-scale, we see that also Only LC (right) performs worse compared to the regularized two stage approaches.

only identifies most, but not all, of the zero and non-zero βs correctly (see Figure 30). Only the regularized two stage approaches are able to recover the true causal βs.

F.2 Setting B

In this part we will examine the methods for Setting B eq. (5). Note that the first stage is misspecified for the two stage approaches, whereas the second stage is wellspecified for all methods.

F.2.1 Setting B with $p = 3, q = 2$

Even in this low-dimensional scenario, DIR+LC suffers substantially from the misspecified second stage. It is not able to produce sensible estimates. We argue that this might be due to the "forbidden regression" issue. Furthermore, the naive regression is highly influenced by confounding. It even flips the estimated effect of two components, see Figure 34. Nevertheless the remaining two stage methods, except 2SLS which ignores compositionality, perform
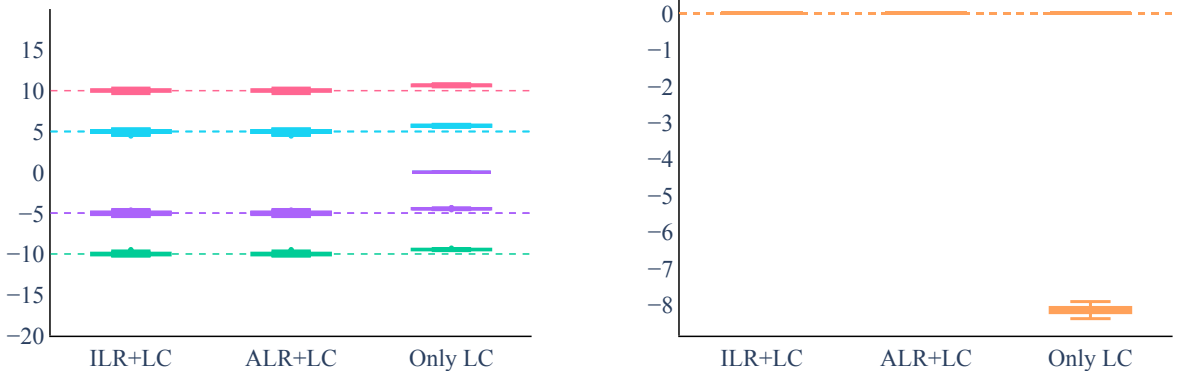
Figure 32: **Setting A with** $p = 250$, $q = 10$: The boxplots show the $\hat{\beta}$ values for the 50 runs for each of the 8 non-zero β coefficients (dashed lines, left) and the 242 zero β coefficients (dashed line, right). The two stage methods are able to recover the causal effect on average, whereas the naive regression method is not able to recover the true support. 2SLS_{ILR} does not produce sensible estimates due to the missing regularization and is omitted for better readability.
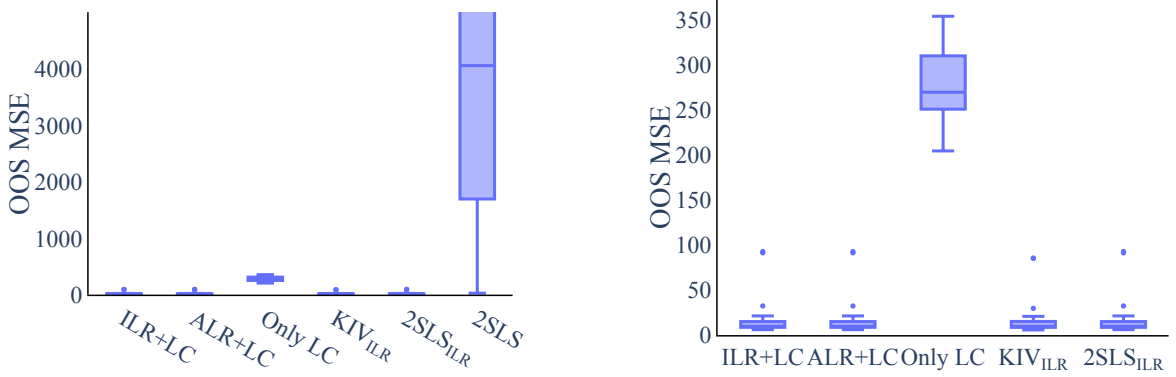
Figure 33: **Setting B with** $p = 3$, $q = 2$: The boxplots show the OOS MSE of 20 runs. 2SLS and DIR+LC perform way worse as compared to the two stage approaches (left). When we adjust the y-scale (right), Only LC also cannot compare to the remaining two-stage approaches. ALR+LC, ILR+LC, 2SLS_{ILR} are equivalent in the low-dimensional case.

reasonably well in recovering the true causal effect (see Figure 33).

F.2.2 Setting B with $p = 30, q = 10$

Microbiome compositional data is typically high-dimensional and comprises many zero values. Moreover, it is often assumed that only a few microbial compositions (and hence β parameters) influence an outcome of interest Y. Thus, in the following, we will emulate such a scenario and assume a sparse β as ground truth and additionally—as ZINegBinom can incorporate sparsity also on X—run the models on relatively sparse X (see Appendix D).

Note that for higher-dimensional approaches, we omit results for DIR+LC due to computational issues stemming from the maximum likelihood estimation of the α_0 and α parameters in the first stage.

Moreover, for $p = 30$, 2SLS_{ILR} already is unfit to capture the causal effect due to missing regularization. Due to its high OOS MSE value, we omitted 2SLS_{ILR} in Figure 36 for better readability. 2SLS, which ignores the compositionality of X altogether, is able to converge,
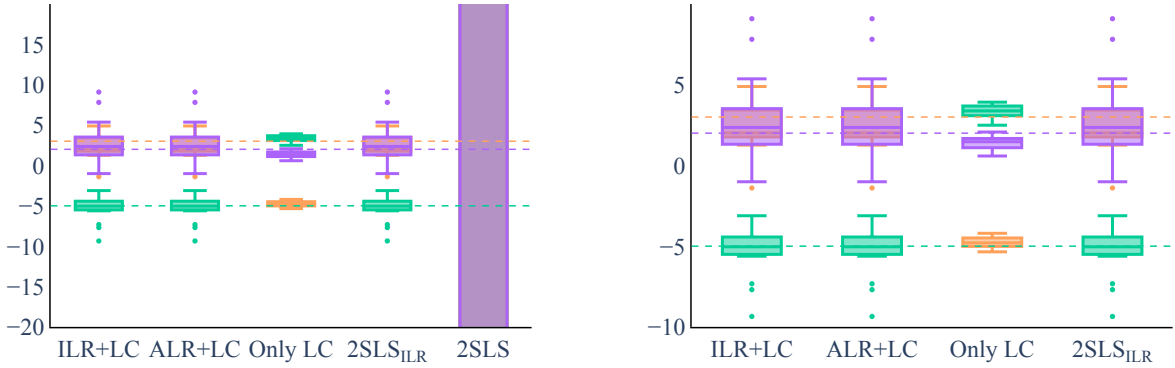
Figure 34: **Setting B with** $p = 3$, $q = 2$: The boxplots show the $\hat{\beta}$ values for the 20 runs for each of the 3 β coefficients. The two stage methods (except for DIR+LC and 2SLS) are able to recover the true causal βs on average. However, when we adjust the y-scale (right), the problem of confounding becomes apparent: Only LC flips the sign of two of the non-zero β values.
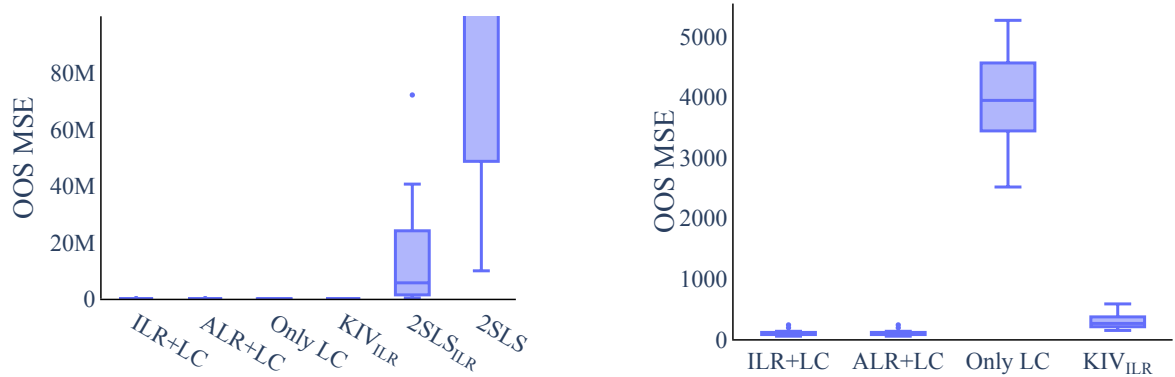

Figure 35: **Setting B with** $p = 30$, $q = 10$: The boxplots show the OOS MSE of 20 runs. $2SLS_{ILR}$ is only reasonable in low-dimensions (left). When we adjust the y-scale (right), we see that the remaining two-stage approaches outperform the naive regression.

but does not produce reasonable estimates.

For KIV_{ILR}, the difficulty of tuning the method in higher dimensions remains an issue (see Figure 35). The remaining two stage approaches, however, benefit substantially from the instrumentation of X by Z. They outperform the naive regression both on OOS MSE (see Figure 35), as well as on the recovery of the true β values (see Figure 36). While the naive regression not only fails to recover the true β values, it also produces quite volatile estimates (see Figure 36).

F.2.3   Setting B with $p = 250, q = 10$

Microbiome compositional data is typically high-dimensional and comprises many zero values. Moreover, it is often assumed that only a few microbial compositions (and hence β parameters) influence an outcome of interest Y. Thus, in the following, we will emulate such a scenario and assume a sparse β as ground truth and additionally—as ZINegBinom can incorporate sparsity also on X—run the models on relatively sparse X (see Appendix D).

Note that for higher-dimensional approaches, we omit results for DIR+LC due to computational issues stemming from the maximum likelihood estimation of the α_0 and α parameters
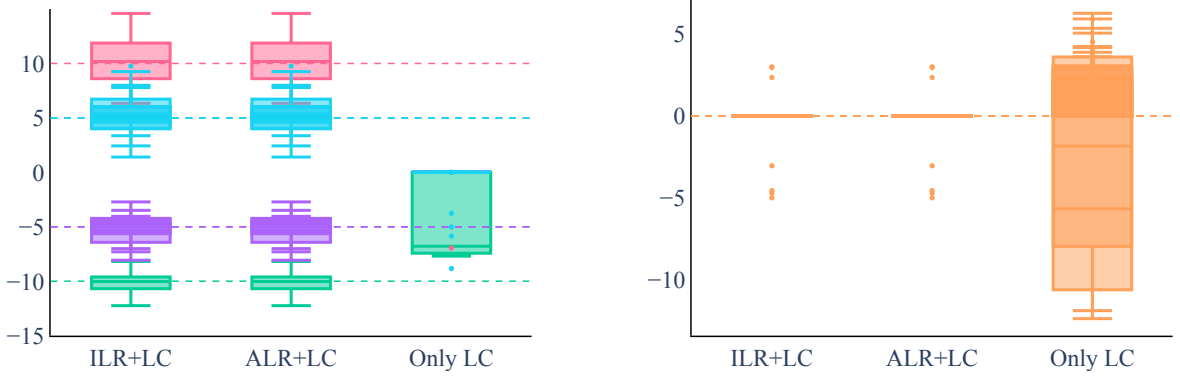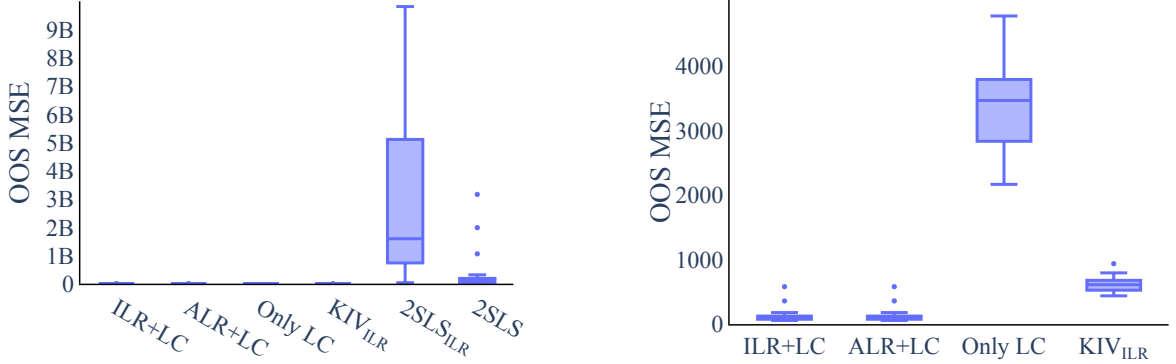
Figure 36: **Setting B with** $p = 30$, $q = 10$: The boxplots show the $\hat{\beta}$ values for the 20 runs for each of the 8 non-zero β coefficients (dashed lines, left) and the 22 zero β coefficients (dashed line, right). The naive regression Only LC is not able to recover the β values at all. ILR+LC and ALR+LC are better suited to recover the causal parameters when confounding is present. Despite the misspecified first stage, they are able to recover the causal β values on average.

Figure 37: **Setting B with** $p = 250$, $q = 10$: The boxplots show the OOS MSE of 20 runs. $2SLS_{ILR}$ is only reasonable in low-dimensions and KIV_{ILR} is difficult to tune in higher dimensions (left). When we adjust the y-scale (right), we see that ILR+LC and ALR+LC outperform the naive regression.

in the first stage.

Both high-dimensional scenarios generally agree in their outcomes; for $p = 250$ the short-comings of the different approaches only get more enhanced.

While 2SLS, which ignores the compositionality of X altogether, is also able to converge for $p = 250$, it does not produce reasonable estimates. Further, the regularized two stage methods still perform reasonably well, while $2SLS_{ILR}$ and KIV_{ILR} cannot match that performance (see Figure 37) due to the lack of sensible regularization. The naive approach can capture neither the causal effect nor the causal β values (see Figure 37 and Figure 38).

F.3 Further settings for robustness estimation

We will analyze the results form our "robustness" scenarios including a weak instrument setting and a setting with a nonlinear functional relationship in the second stage.
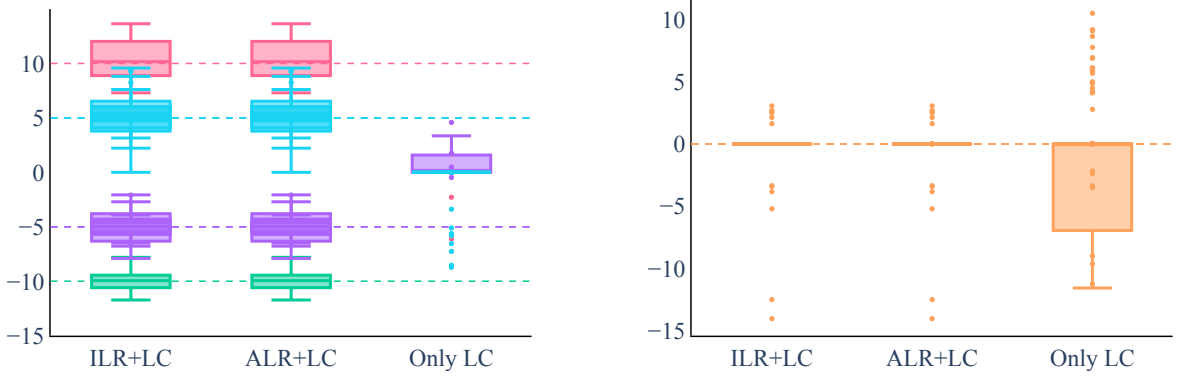
Figure 38: **Setting B with** $p = 250$**,** $q = 10$**:** The boxplots show the $\hat{\beta}$ values for the 20 runs for each of the 8 non-zero β coefficients (dashed lines, left) and the 242 zero β coefficients (dashed line, right). Only LC is not able to recover the β values at all. ILR+LC and ALR+LC are better suited to recover the causal parameters even when confounding is present. Despite the misspecified first stage, they are able to recover the causal β values on average.

F.3.1 Weak instrument(s)

Setting A with $p = 3, q = 2$ **and weak instruments**   In a strong/valid instrument setting, two stage methods have a clear advantage. To test the limitations of our methods, we now analyze an equivalent setting with a comparatively weak instrument. In this setting, confounding is still noticeable (see Figure 21) but the first stage F-statistic is much lower, indicating that we may suffer from weak instrument bias.

The two stage methods have a higher variation in their estimates, both for OOS MSE and $\hat{\beta}$ (see Figure 39 and Figure 40), whereas the naive regression does not change at all (since only the first stage data generation has changed). Nevertheless, the wellspecified two stage methods (ALR+LC, ILR+LC, 2SLS$_{\text{ILR}}$) still recover the causal effects better than the naive regression. Only the DIR+LC regression runs into problems due to two misspecified stages. We thus conclude that the "forbidden regression" is not necessarily detrimental to cause-effect estimation when the instrument is strong, but can indeed result in unreliable results for weaker instruments.

F.3.2 Nonlinear second stage

Setting A with $p = 3, q = 2$ **and a non-linear function form of** f The two stage methods perform well if they are in a wellspecified setting. With the DIR+LC method, however, it becomes obvious that misspecification can become problematic. Furthermore, wellspecification is typically impossible to ascertain in practice and most real-world examples are likely not perfectly linear. Thus, we add a polynomial X dependency term in the second stage to evaluate ALR+LC, ILR+LC and 2SLS$_{\text{ILR}}$ on a partly misspecified setting.

Note that we can only look at the OOS MSE as the β values do not carry any causal interpretation (see Figure 41). The DIR+LC still suffers from two misspecified stages and performs worst. When only the second stage is misspecified, ALR+LC, ILR+LC and 2SLS$_{\text{ILR}}$ still outperform the naive regressions. However, we are not able to capture the true causal effect because of the misspecification in the second stage. The overall error thus grows in all methods.
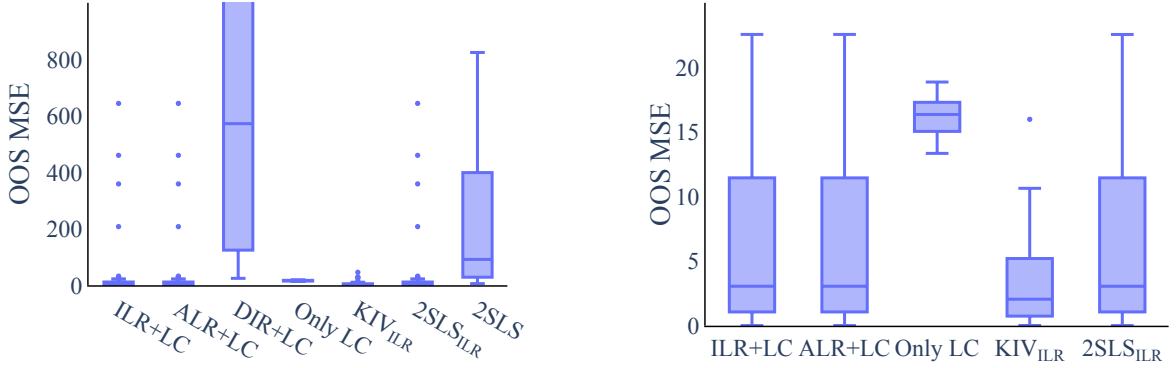
43

Figure 39: **Setting A with** $p = 3$, $q = 2$ **and weak instruments:** The boxplots show the OOS MSE of 50 runs. The DIR+LC performs considerably worse than all the other methods. The problem might stem from the "forbidden regression" issue coming from two misspecified stages. On the right hand side we adjusted the y-scale. The graph shows that the other wellspecified methods still outperform the naive regression in terms of OOS MSE in the weak instrument setting. We observe a higher variance in performance than in the stronger instrument setting.
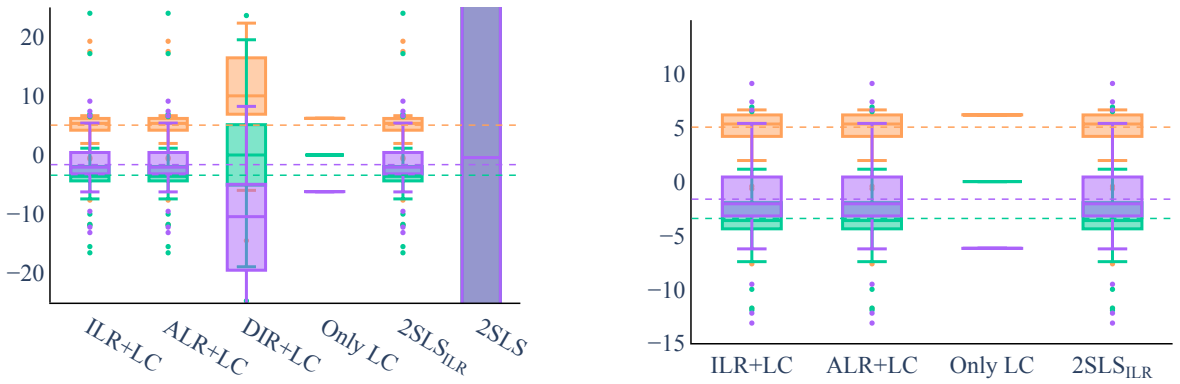

Figure 40: **Setting A with** $p = 3$, $q = 2$ **and weak instruments:** The boxplots show the $\hat{\beta}$ values for the 50 runs for each of the 3 β coefficients (dashed lines). In the weaker instrument setting, we are able to recover the true β values for the wellspecified two stage methods, even though the variance of the $\hat{\beta}$ is higher while the naive regression is still subject to confounding (right, zoomed in plot). Only the DIR+LC is not able to recover the causal effect and seems biased toward the naive regression (left). This might be due to two misspecified stages.
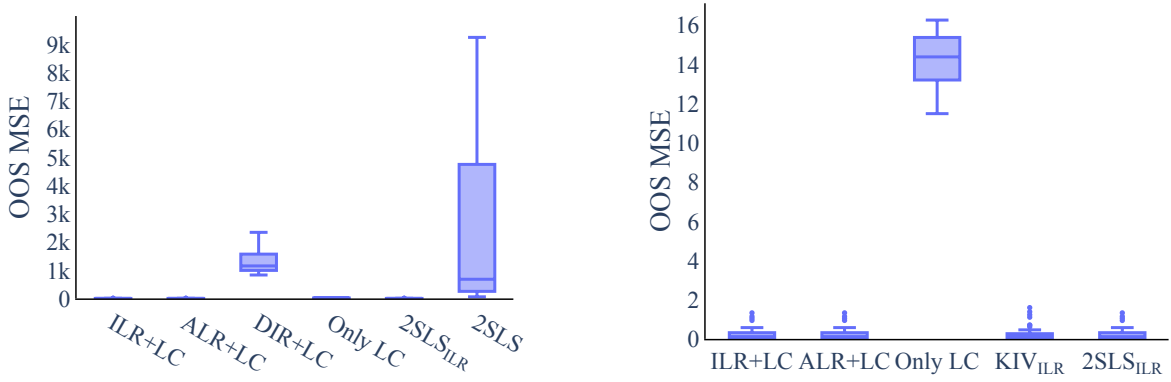
44

Figure 41: **Setting A with** $p = 3$, $q = 2$ **and a non-linear function form of** f: The boxplots show the OOS MSE of 50 runs. DIR+LC and 2SLS perform worst (left). The other two stage approaches are able to recover the causal effect better than the naive regression. The correctly specified first stage helps in filtering out the confounding effect in the two stage methods.

F.4 Real data example

We return to the real data of (Schulfer et al., 2019).

This is a more detailed examination of the real data example given in the main part. We provide results on further aggregation levels, resp. 'Order' and 'Family'. Moreover, we discretize the weight outcome Y and replace the squared loss of the log-contrast regression by a Hinge loss (see Appendix E).

We shortly recap the generation of the dataset and the justification of the instrumental variable setting: a total of 57 new born mice were assigned randomly to a sub-therapeutic antibiotic treatment (STAT) during their early stages of development. We have 35 mice in the treatment group and 22 mice in the control group. After 21 days, the gut microbiome composition of each mouse was recorded. We are interested in the causal effect of the gut microbiome composition $X \in \mathbb{S}^{p-1}$ on body weight $Y \in \mathbb{R}$ of the mice (at sacrifice).

We assume a valid instrument due to the following characteristics in the data generation:

1. The random assignment of the antibiotic treatment ensures independence of potential confounders such as genetic factors ($Z \perp\!\!\!\perp U$).

2. The sub-therapeutic dose implies that antibiotics can not be detected in the mice' blood, providing reason to assume no effect of the antibiotics on the weight other than through its effect on the gut microbiome ($Z \perp\!\!\!\perp Y | \{U, X\}$). We remark however, that the effect of Z on X is at least not strong enough to draw statistically significant conclusions.

3. Finally, we observe empirically, that there are statistically significant differences of microbiome compositions between the treatment and control groups ($Z \not\!\perp\!\!\!\perp X$).

Thus we conclude that the assignment of sub-therapeutic antibiotic treatment is a good candidate for an instrumental variable Z.

For the log-contrast regression we applied a threshold of 0.65 both for the continuous as well as for the categorical outcome Y.
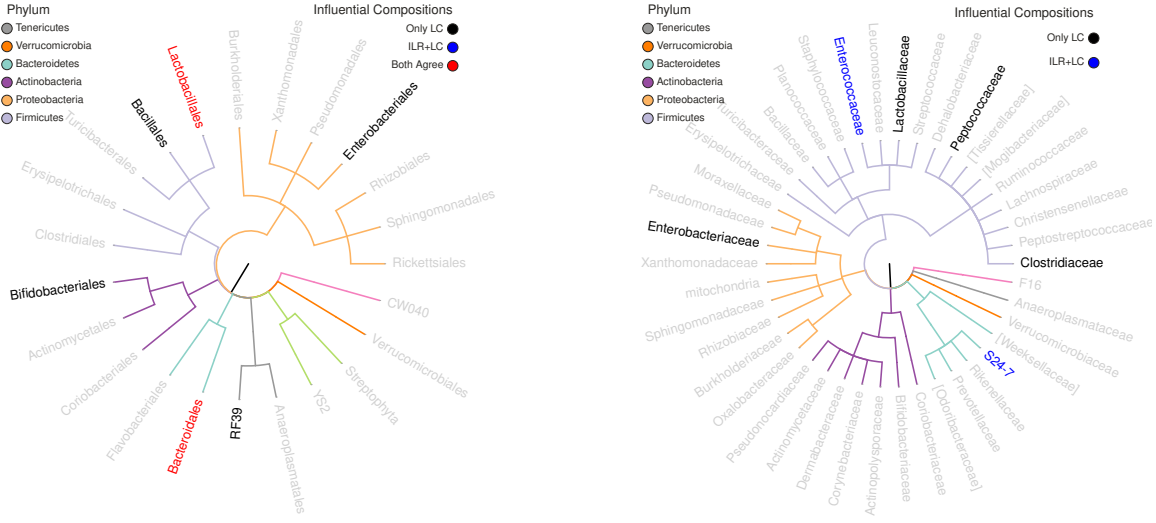
Figure 42: **Influential Compositions on Order Level (left) and Family Level (right):** On order level, both methods agree on one influential log ratio. For the family level, there is a divide between the two-stage method and the naive regression. This could suggest that Only LC is subject to confounding on the corresponding aggregation level.

F.4.1 Further results on different aggregation levels

Naturally, for real data, we do not have ground truth labels available. However, the importance of being able to draw causal and actionable conclusions becomes apparent. In the main part we provide the results for the naive regression and the two-stage method ILR+LC on genus level. The methods did not agree on the influential log-ratios, thus suggesting that Only LC might be subject to confounding. This result also holds true on family level. However, on order level both methods detect one common log-ratio (see Figure 42).

F.4.2 Categorical/binary outcome

In order to provide a more complete picture of the loss possibilities, we include results for a categorical/binary Y.

Originally, the real data includes weight measured in gram. To create a binary outcome, we split the data by the mean of the outcome Y thus artificially generating an "underweight" population of 29 mice and an "overweight" population of 28 mice.

Again, we show the influential log-ratios for the naive regression Only LC and ILR+LC (see Figure 43). While for ILR+LC the influential log-ratios stay the same for binary and continuous outcome, for the naive regression they are not entirely consistent.
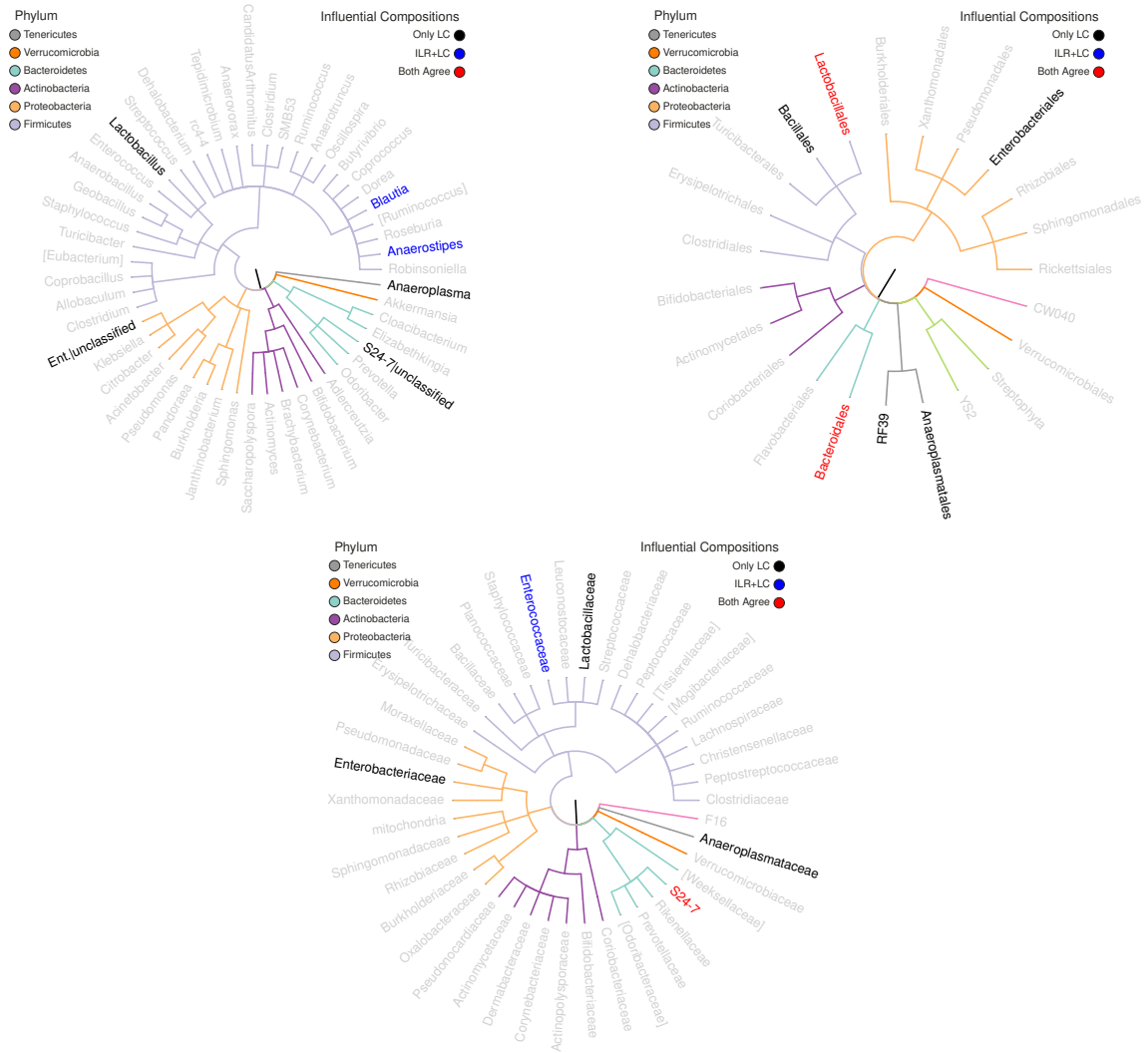
Figure 43: **Influential Compositions on Genus Level (top left), Order Level (top right) and Family Level (bottom):** In general, the results stay the same for ILR+LC in the binary case and the continuous case. The influential log-ratios are slightly shifting when simply applying a naive regression.